Inorganic Chemistry

Article

pubs.acs.org/IC

Dinuclear Complexes Containing Linear M−F−M [M = Mn(II), Fe(II), Co(II), Ni(II), Cu(II), Zn(II), Cd(II)] Bridges: Trends in Structures, Antiferromagnetic Superexchange Interactions, and Spectroscopic Properties

Daniel L. Reger,*[,†] Andrea E. Pascui,[†] Mark D. Smith,[†] Julia Jezierska,[‡] and Andrew Ozarowski*[,§]

[†]Department of Chemistry and Biochemistry, University of South Carolina, Columbia, South Carolina 29208, United States

[‡]Faculty of Chemistry, University of Wrocław, 50-383 Wrocław, Poland

[§]National High Magnetic Field Laboratory, Florida State University, Tallahassee, Florida 32310, United States

Supporting Information

ABSTRACT: The reaction of $M(BF_4)_2 \cdot xH_2O$, where M is Fe(II), Co(II), Ni(II), Cu(II), Zn(II), and Cd(II), with the new ditopic ligand *m*-bis[bis(3,5-dimethyl-1-pyrazolyl)-methyl]benzene ($\mathbf{L}_m$*) leads to the formation of mono-fluoride-bridged dinuclear metallacycles of the formula $[M_2(\mu\text{-}F)(\mu\text{-}\mathbf{L}_m^*)_2](BF_4)_3$. The analogous manganese(II) species, $[Mn_2(\mu\text{-}F)(\mu\text{-}\mathbf{L}_m^*)_2](ClO_4)_3$, was isolated starting with $Mn(ClO_4)_2 \cdot 6H_2O$ using $NaBF_4$ as the source of the bridging fluoride. In all of these complexes, the geometry around the metal centers is trigonal bipyramidal, and the fluoride bridges are linear. The ^1H, ^{13}C, and ^{19}F NMR spectra of the zinc(II) and cadmium(II) compounds and the ^{113}Cd NMR of the cadmium(II) compound indicate that the metallacycles retain their structure in acetonitrile and acetone solution. The compounds with M = Mn(II), Fe(II), Co(II), Ni(II), and Cu(II) are antiferromagnetically coupled, although the magnitude of the coupling increases dramatically with the metal as one moves to the right across the periodic table: Mn(II) (-6.7 cm^{-1}) < Fe(II) (-16.3 cm^{-1}) < Co(II) (-24.1 cm^{-1}) < Ni(II) (-39.0 cm^{-1}) ≪ Cu(II) (-322 cm^{-1}). High-field EPR spectra of the copper(II) complexes were interpreted using the coupled-spin Hamiltonian with $g_x = 2.150$, $g_y = 2.329$, $g_z = 2.010$, $D = 0.173$ cm^{-1}, and $E = 0.089$ cm^{-1}. Interpretation of the EPR spectra of the iron(II) and manganese(II) complexes required the spin Hamiltonian using the noncoupled spin operators of two metal ions. The values $g_x = 2.26$, $g_y = 2.29$, $g_z = 1.99$, $J = -16.0$ cm^{-1}, $D_1 = -9.89$ cm^{-1}, and $D_{12} = -0.065$ cm^{-1} were obtained for the iron(II) complex and $g_x = g_y = g_z = 2.00$, $D_1 = -0.3254$ cm^{-1}, $E_1 = -0.0153$, $J = -6.7$ cm^{-1}, and $D_{12} = 0.0302$ cm^{-1} were found for the manganese(II) complex. Density functional theory (DFT) calculations of the exchange integrals and the zero-field splitting on manganese(II) and iron(II) ions were performed using the hybrid B3LYP functional in association with the TZVPP basis set, resulting in reasonable agreement with experiment.

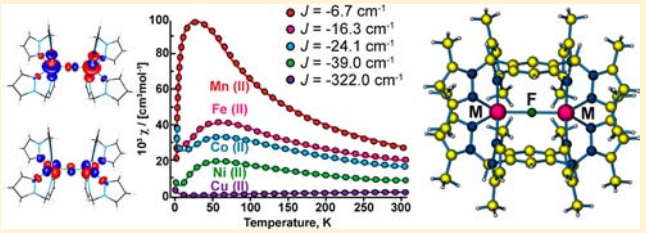

INTRODUCTION

A major emphasis in inorganic chemistry is the preparation of new ligands that are designed to control the structures of metal complexes.[1] Much of our research is centered on the use of designed "third-generation" poly(pyrazolyl)methane ligands.[2] Whereas "second-generation" poly(pyrazolyl)methane ligands control the metal coordination site with bulky groups located near the pyrazolyl nitrogen donor,[3] third-generation poly-(pyrazolyl)methane ligands control the overall structure by specific functionalization at the noncoordinating "back" position. An important class of these types of ligands links multiple poly(pyrazolyl)methane units into a single molecule. This linkage can be made with either flexible[2b,4] or fixed[5] central groups. Within the latter case of ligands, we have demonstrated that linking two bis(pyrazolyl)methane units through a meta-substituted arene spacer triggers the formation of dinuclear metallacycles.[6]

Using the fixed ligand *m*-bis[bis(1-pyrazolyl)methyl]benzene (*m*-$[CH(pz)_2]_2C_6H_4$, $\mathbf{L}_m$, pz = pyrazolyl ring; Scheme 1), we have reported the syntheses of dinuclear metallacycles with silver(I)[6a] and, in the case of higher-charged first-row metals

Scheme 1. Schematic Drawings of *m*-$[CH(pz)_2]_2C_6H_4$ ($\mathbf{L}_m$) and *m*-$[CH(3,5\text{-dimethyl-1-pz})_2]_2C_6H_4$ ($\mathbf{L}_m$*)

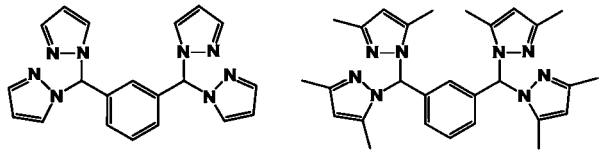

$\mathbf{L}_m$ $\mathbf{L}_m$*

Received: August 10, 2012
Published: October 9, 2012

   dx.doi.org/10.1021/ic301757g | *Inorg. Chem.* 2012, 51, 11820−11836

iron(II), cobalt(II), copper(II), and zinc(II), metallacyclic complexes of the formula $[M_2(\mu\text{-}F)(\mu\text{-}\mathbf{L}_m)_2]^{3+}$, which contain a linear or nearly linear bridging fluoride that arises from abstraction from tetrafluoroborate (BF_4^-).[6b,c] Such a metallacycle is exemplified by the fluoride-bridged iron(II) compound shown in Figure 1. With nickel(II) and cadmium(II),

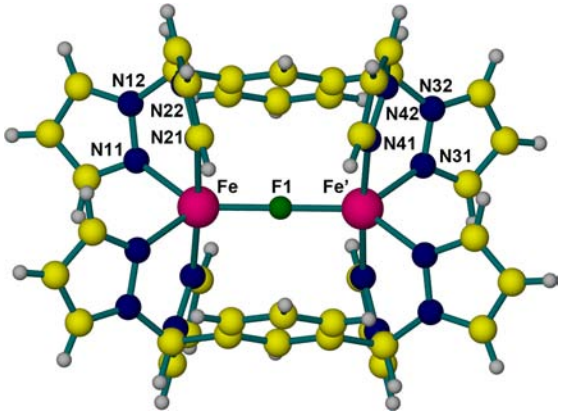

Figure 1. Structure of $[Fe_2(\mu\text{-}F)(\mu\text{-}\mathbf{L}_m)_2]^{3+}$.

difluoride-bridged complexes form. Although there were a number of examples of fluoride-bridged[7] compounds in the literature, our monobridged compounds represent an almost unknown structural type and offer a unique opportunity to prepare and investigate the properties of a series of complexes with similar structures where the metal can be extensively varied. We are particularly interested in the magnetic properties of these complexes because theory[8] indicates that linear M−F−M fluoride bridges (and other bridges such as OH^- and Cl^-) would yield complexes that show strong intramolecular antiferromagnetic exchange interactions. In our initial work[6b,c] with $\mathbf{L}_m$, such strong antiferromagnetic properties were observed for the copper(II) complex, but only weakly antiferromagnetic properties were observed for the iron(II) and cobalt(II) complexes, and we were unable to prepare a monobridged nickel(II) complex for comparison.

As reported here, we have determined that the new ligand *m*-bis[bis(3,5-dimethyl-1-pyrazolyl)methyl]benzene ($\mathbf{L}_m$*, Scheme 1) forms a series of monobridged fluoride complexes with first-row transition metals from manganese(II) to zinc(II) and also cadmium(II) that all have linearly bridged monofluoride metallacyclic structures, the first extensive series of complexes with this bridging structural motif. Crystallographic, magnetic and EPR studies and DFT calculations of the paramagnetic complexes $[M_2(\mu\text{-}F)(\mu\text{-}\mathbf{L}_m^*)_2](A)_3$ [M = Mn(II), Fe(II), Co(II), Ni(II), Cu(II), A = BF_4^- or ClO_4^-] allowed for a careful comparison of the effects of the metal ions on the structure and magnetic and EPR properties of these linearly fluoride-bridged complexes. The zinc(II) and cadmium(II) complexes provide interesting NMR data. We have previously communicated information on $[Cu_2(\mu\text{-}F)(\mu\text{-}\mathbf{L}_m^*)_2](ClO_4)_3$.[9]

EXPERIMENTAL SECTION

General Considerations. For the synthesis of the fluoride-bridged compounds, standard Schlenk techniques were used. The solvents for the syntheses of metal complexes were not dried prior to use. The metal tetrafluoroborates and the manganese(II) perchlorate were purchased from Sigma-Aldrich or Strem Chemicals and were used as received. Reported melting points are uncorrected.

Crystals used for elemental analysis and mass spectrometry were removed from the mother liquor, rinsed with ether, and dried under a vacuum, a process that removes solvent of crystallization, if present.

^1H, ^{13}C, ^{19}F, and ^{113}Cd NMR spectra were recorded on a Varian Mercury/VX 300, Varian Mercury/VX 400, or Varian INOVA 500 spectrometer. All chemical shifts are in parts per million (ppm) and were referenced to residual undeuterated solvent signals (^1H), deuterated solvent signals (^{13}C), or externally to $CFCl_3$ (^{19}F) or $CdCl_2$ (^{113}Cd). Mass spectrometric measurements were obtained on a MicroMass QTOF spectrometer in an acid-free environment. Elemental analyses were performed on vacuum-dried samples by Robertson Microlit Laboratories (Ledgewood, NJ).

High-field, high-frequency EPR spectra at temperatures ranging from ca. 6 to 290 K were recorded on a home-built spectrometer at the EMR facility of the NHMFL.[10] The instrument is a transmission-type device in which microwaves are propagated in cylindrical lightpipes. The microwaves were generated by a phase-locked Virginia Diodes source generating a frequency of 13 ± 1 GHz and producing its harmonics of which the 2nd, 4th, 6th, 8th, 16th, 24th, and 32nd were available. A superconducting magnet (Oxford Instruments) capable of reaching a field of 17 T was employed. The powder samples were not constrained and showed no magnetic torquing at high magnetic fields.

Magnetic susceptibility measurements over the temperature range from 1.8 to 300 K were performed at a magnetic field of 0.5 T using a Quantum Design SQUID MPMSXL-5 magnetometer. Correction for the sample holder and the diamagnetic correction χ_D, which was estimated from the Pascal constants,[11] were applied.

XSEED, POV-RAY, MESTRENOVA, and GOpenMol were used for the preparation of figures.[12]

***m*-Bis[bis(3,5-dimethyl-1-pyrazolyl)methyl]benzene (*m*-[CH-(3,5-Me$_2$pz)$_2$]$_2$C$_6$H$_4$, $\mathbf{L}_m$*).** Under a nitrogen atmosphere, a 500 mL Schlenk flask containing sodium hydride (3.90 g, 163 mmol) suspended in anhydrous tetrahydrofuran (THF; 350 mL) was cooled in an ice bath for 30 min. Solid 3,5-dimethylpyrazole (15.67 g, 163 mmol) was added over 10 min, and the resulting solution was allowed to stir at 0 °C for 30 min. After the dropwise addition of thionyl chloride (5.94 mL, 81.4 mmol), the ice bath was removed, and the suspension was allowed to warm to room temperature over 30 min. Isophthalaldehyde (2.73 g, 20.4 mmol) and anhydrous $CoCl_2$ (0.26 g, 2.0 mmol) were added at once, and the reaction mixture was heated at reflux for 42 h. After the mixture had cooled to room temperature, water (160 mL) was added, and the resulting solution was left to stir for 30 min. The organic and aqueous layers were separated, and the aqueous layer was extracted with CH_2Cl_2 (2 × 100 mL). The combined organic extracts were washed with water (100 mL) and dried over $MgSO_4$. Removal of the solvent left a beige solid containing unreacted 3,5-dimethylpyrazole, which was removed by sublimation at 70−80 °C under vacuum for 2 days. The remaining solid was dissolved in ethyl acetate and flushed through a plug of silica. Removal of solvent afforded 8.02 g (81%) of white product, melting point 152−153 °C. ^1H NMR (300 MHz, acetone-d_6): δ 7.67 [s, 2H, CH(3,5-pz)$_2$], 7.37 (t, J = 6.0 Hz, 1H, 5-H C$_6$H$_4$), 6.97 (d, J = 9.0 Hz, 2H, 4,6-H C$_6$H$_4$), 6.57 (s, 1H, 2-H C$_6$H$_4$), 5.84 (s, 4H, 4-H 3,5-pz), 2.18/2.09 (s/s, 12H/12H, 3,5-CH$_3$). ^{13}C NMR (75.5 MHz, acetone-d_6): δ 148.3/141,6 (3,5-C pz), 138.3 (1,3-C C$_6$H$_4$), 129.0 (5-C C$_6$H$_4$), 127.8 (4,6-C C$_6$H$_4$), 126.9 (2-C C$_6$H$_4$), 107.22 (4-C pz), 74.4 [CH(pz)$_2$], 13.69/11.80 (CH$_3$). Anal. Calcd (found) for $C_{28}H_{34}N_8$: C, 69.68 (69.37); H, 7.10 (7.40); N, 23.22 (23.05). MS ES(+) m/z (relative percent abundance) [assignment]: 521 (28) [$\mathbf{L}_m$* + K]$^+$, 505 (92) [$\mathbf{L}_m$* + Na]$^+$, 483 (100) [$\mathbf{L}_m$* + H]$^+$, 387 (70) [$\mathbf{L}_m$* − 3,5-Me$_2$pz]$^+$. HRMS ES$^+$ (m/z): [$\mathbf{L}_m$*+ H]$^+$ calcd for $[C_{28}H_{35}N_8]^+$ 483.2984; found 483.2988.

[Fe$_2$(μ-F)(μ-$\mathbf{L}_m$)$_2$](BF$_4$)$_3$ (**1**).* Both $\mathbf{L}_m$* (0.241 g, 0.50 mmol) and $Fe(BF_4)_2{\cdot}6H_2O$ (0.169 g, 0.50 mmol) were separately dissolved in THF (10 mL), and the ligand solution was transferred by cannula into the iron solution. An off-white precipitate formed immediately. The reaction mixture was stirred for 5 h, after which time the system was cannula filtered, and the remaining solid was washed with THF (10

dx.doi.org/10.1021/ic301757g | Inorg. Chem. 2012, 51, 11820−11836

Table 1. Selected Crystal Data and Structure Refinement

	1	2	3·2H$_2$O	4	4	5·2H$_2$O	6·2CH$_3$CN	7·2CH$_3$CN
formula	C_{56} H_{68} B_3 F_{13} N_{16} Fe_2	C_{56} H_{68} B_3 F_{13} N_{16} Co_2	C_{56} H_{72} B_3 F_{13} N_{16} O_2 Ni_2	C_{56} H_{68} B_3 F_{13} N_{16} Cu_2	C_{56} H_{68} B_3 F_{13} N_{16} Cu_2	C_{56} H_{72} B_3 F_{13} N_{16} O_2 Zn_2	C_{60} H_{74} B_3 F_{13} N_{18} Cd_2	C_{60} H_{74} Cl_3 F N_{18} O_{12} Mn_2
Fw (g·mol^{-1})	1356.39	1362.55	1398.15	1371.77	1371.77	1411.47	1551.60	1474.60
crystal syst	triclinic	triclinic	monoclinic	triclinic	triclinic	monoclinic	monoclinic	monoclinic
space group	$P\bar{1}$	$P\bar{1}$	$P2_1/n$	$P\bar{1}$	$P1$	$P2_1/n$	$C2/c$	$P2_1/n$
T (K)	296(2)	296(2)	150(2)	296(2)	150(2)	150(2)	100(2)	100(2)
a (Å)	11.1007(4)	11.1049(13)	14.5757(9)	11.223(4)	12.5765(8)	14.6112(8)	18.0575(8)	22.1885(11)
b (Å)	12.7715(5)	12.7328(15)	13.4631(8)	12.712(4)	13.5961(9)	13.5709(8)	18.7759(8)	14.1645(7)
c (Å)	13.4497(5)	13.3656(15)	15.9731(9)	13.453(4)	27.8253(18)	15.9646(9)	20.6046(9)	22.5076(11)
α (deg)	117.203(1)	116.666(2)	90	116.453(6)	82.997(1)	90	90	90
β (deg)	99.415(1)	99.639(2)	95.171(1)	101.258(6)	88.741(1)	95.154(1)	100.845(1)	106.512(1)
γ (deg)	104.248(1)	104.647(2)	90	103.926(6)	71.763(1)	90	90	90
V (Å^3)	1557.13(10)	1545.3(3)	3121.7(3)	1563.6(9)	4484.5(5)	3152.8(3)	6861.1(5)	6782.2(6)
Z	1	1	2	1	3	2	4	4
R1 [$I > 2\sigma(I)$]	0.0549	0.0532	0.0364	0.0627	0.0480	0.0361	0.0349	0.0391
wR2 [$I > 2\sigma(I)$]	0.1497	0.1549	0.0876	0.1677	0.1167	0.0893	0.0970	0.0989

mL) and dried under a vacuum overnight, affording 0.326 g (96%) of the crude product. Single crystals suitable for X-ray studies were grown by the vapor diffusion of Et_2O into 1 mL of an acetonitrile solution (20 mg/mL) of **1**. Anal. Calcd (found) for $C_{56}H_{68}B_3Fe_2N_{16}F_{13}$: C, 49.59 (49.75); H, 5.05 (4.81); N, 16.52 (16.75). MS ESI(+) m/z (relative percent abundance) [assignment]: 1269 (25) $[Fe_2(\mathbf{L}_m^*)_2F(BF_4)_2]^+$, 591 (48) $[Fe_2(\mathbf{L}_m^*)_2F(BF_4)]^{2+}$, 557 (87) $[Fe\mathbf{L}_m^*F]^+$, 483 (12) $[\mathbf{L}_m^* + H]^+$, 365 (100) $[Fe_2(\mathbf{L}_m^*)_2F]^{3+}$. HRMS ES$^+$ (m/z): $[Fe_2(\mathbf{L}_m^*)_2F(BF_4)_2]^+$ calcd for $[C_{56}H_{68}B_2Fe_2F_9N_{16}]^+$ 1269.4575; found 1269.4519.

*$[Co_2(\mu\text{-}F)(\mu\text{-}\mathbf{L}_m^*)_2](BF_4)_3$ (**2**).* Compound **2** was prepared similarly to compound **1** starting from $Co(BF_4)_2{\cdot}6H_2O$ (0.170 g, 0.5 mmol). The reaction afforded 0.310 g of a pink solid (91%). Single crystals suitable for X-ray studies were grown by the vapor diffusion of Et_2O into 1 mL of an acetonitrile solution (30 mg/mL) of **2**. Anal. Calcd (found) for $C_{56}H_{68}B_3Co_2N_{16}F_{13}$: C, 49.37 (49.23); H, 5.03 (4.83); N, 16.45 (16.55). MS ESI(+) m/z (relative percent abundance) [assignment]: 1275 (28) $[Co_2(\mathbf{L}_m^*)_2F(BF_4)_2]^+$, 594 (50) $[Co_2(\mathbf{L}_m^*)_2F(BF_4)]^{2+}$, 560 (80) $[Co\mathbf{L}_m^*F]^+$, 483 (5) $[\mathbf{L}_m^* + H]^+$, 367 (100) $[Co_2(\mathbf{L}_m^*)_2F]^{3+}$. HRMS ES$^+$ (m/z): $[Co_2(\mathbf{L}_m^*)_2F(BF_4)_2]^+$ calcd for $[C_{56}H_{68}B_2Co_2F_9N_{16}]^+$ 1275.4486; found 1275.4537.

*$[Ni_2(\mu\text{-}F)(\mu\text{-}\mathbf{L}_m^*)_2](BF_4)_3$ (**3**).* Compound **3** was prepared similarly to compound **1** starting from $Ni(BF_4)_2{\cdot}6H_2O$ (0.170 g, 0.5 mmol). The reaction afforded 0.280 g of crude product (82%). Compound **3** was crystallized as compound **2** and was taken directly from the mother liquor for crystallographic studies as **3**·2H$_2$O. Anal. Calcd (found) for $C_{56}H_{68}B_3Ni_2N_{16}F_{13}$: C, 49.38 (49.27); H, 5.03 (4.81); N, 16.45 (16.62). MS ESI(+) m/z (relative percent abundance) [assignment]: 1273 (10) $[Ni_2(\mathbf{L}_m^*)_2F(BF_4)_2]^+$, 593 (50) $[Ni_2(\mathbf{L}_m^*)_2F(BF_4)]^{2+}$, 559 (10) $[Ni\mathbf{L}_m^*F]^+$, 366 (100) $[Ni_2(\mathbf{L}_m^*)_2F]^{3+}$. HRMS ES$^+$ (m/z): $[Ni_2(\mathbf{L}_m^*)_2F(BF_4)_2]^+$ calcd for $[C_{56}H_{68}B_2Ni_2F_9N_{16}]^+$ 1273.4557; found 1273.4583.

*$[Cu_2(\mu\text{-}F)(\mu\text{-}\mathbf{L}_m^*)_2](BF_4)_3$ (**4**).* Compound **4** was prepared similarly to compound **1** starting from $Cu(BF_4)_2{\cdot}3H_2O$ (0.145 g, 0.5 mmol). The reaction afforded 0.245 g of crude product (72%). Compound **4** was crystallized as compound **2**. Anal. Calcd (found) for $C_{56}H_{68}B_3Cu_2N_{16}F_{13}$: C, 49.03 (48.78); H, 5.00 (4.76); N, 16.34 (16.36). MS ESI(+) m/z (relative percent abundance) [assignment]: 1283 (7) $[Cu_2(\mathbf{L}_m^*)_2F(BF_4)_2]^+$, 1028 (18) $[Cu(\mathbf{L}_m^*)_2]^+$, 599 (30) $[Cu_2(\mathbf{L}_m^*)_2F(BF_4)]^{2+}$, 564 (12) $[Cu\mathbf{L}_m^*F]^+$, 545 (100) $[Cu\mathbf{L}_m^*]^+$, 483 (68) $[\mathbf{L}_m^* + H]^+$, 370 (60) $[Cu_2(\mathbf{L}_m^*)_2F]^{3+}$. HRMS ES$^+$ (m/z): $[Cu_2(\mathbf{L}_m^*)_2F(BF_4)_2]^+$ calcd for $[C_{56}H_{68}B_2Cu_2F_9N_{16}]^+$ 1273.4557; found 1273.4583.

*$[Zn_2(\mu\text{-}F)(\mu\text{-}\mathbf{L}_m^*)_2](BF_4)_3$ (**5**).* Compound **5** was prepared similarly to compound **1** starting from $Zn(BF_4)_2{\cdot}5H_2O$ (0.165 g, 0.5 mmol). The reaction afforded 0.287 g of crude product (83%). Single crystals suitable for X-ray studies were grown by the vapor diffusion of Et_2O into 1 mL of a methanol solution of **5** and were taken directly from the mother liquor for the crystallographic studies as **5**·2H$_2$O. ^{1}H NMR (300 MHz, acetonitrile-d_3): δ 7.62 (s, 4H, CH(pz)$_2$), 7.56 (t, J = 8.0 Hz, 2H, 5-H C_6H_4), 7.01 (d, J = 8.0 Hz, 4H, 4,6-H C_6H_4), 6.12/6.06 (s/s, 4H/4H, 4-H pz), 5.02 (s, 2H, 2-H C_6H_4), 2.55/2.37 (s/s, 12H/12H, 5-CH$_3$) 1.68/0.73 (s/s, 12H/12H, 3-CH$_3$). ^{13}C NMR (100.6 MHz, acetonitrile-d_3): δ 154.6/152.1/146.0/145.9 (3,5-C pz), 135.8 (1,3-C C_6H_4), 130.6 (5-C C_6H_4), 129.6 (4,6-C C_6H_4), 126.5 (2-C C_6H_4), 109.9/108.0 (4-C pz), 68.6 [CH(pz)$_2$], 16.9/11.5 (3-CH$_3$), 11.1/11.0 (5-CH$_3$). ^{19}F NMR (376 MHz, acetonitrile-d_3): δ −151 (s, BF_4^-), −173 (s, Zn−F−Zn). Anal. Calcd (found) for $C_{56}H_{68}B_3Zn_2N_{16}F_{13}$: C, 48.90 (49.12); H, 4.98 (4.74); N, 16.29 (16.43). MS ES(+) m/z (relative percent abundance) [assignment]: 1287 (8) $[Zn_2(\mathbf{L}_m^*)_2F(BF_4)_2]^+$, 1115 (8) $[Zn(\mathbf{L}_m^*)_2BF_4]^+$, 1047 (10) $[Zn(\mathbf{L}_m^*)_2F]^+$, 873 (10) $[Zn_2\mathbf{L}_m^*(BF_4)_3]^+$, 565 (70) $[Zn\mathbf{L}_m^*F]^+$, 514 (100) $[Zn(\mathbf{L}_m^*)_2]^{2+}$, 483 (52) $[\mathbf{L}_m^* + H]^+$, 371 (15) $[Zn_2(\mathbf{L}_m^*)_2F]^{3+}$, 273 (55) $[Zn\mathbf{L}_m^*]^{2+}$. HRMS ES$^+$ (m/z): $[Zn_2(\mathbf{L}_m^*)_2F(BF_4)_2]^+$ calcd for $[C_{56}H_{68}B_2Zn_2F_9N_{16}]^+$ 1287.4438; found 1287.4435.

*$[Cd_2(\mu\text{-}F)(\mu\text{-}\mathbf{L}_m^*)_2](BF_4)_3$ (**6**).* Compound **6** was prepared similarly to compound **1** starting from $Cd(BF_4)_2{\cdot}6H_2O$ (0.147 g, 0.514 mmol). The reaction afforded 0.295 g of crude product (78%). Single crystals suitable for X-ray studies were grown by the vapor diffusion of Et_2O into 1 mL of an acetonitrile solution of **6** and were taken directly from the mother liquor for crystallographic studies as **6**·2CH$_3$CN. ^{1}H NMR (300 MHz, acetone-d_6): δ 8.03 [s, 4H, CH(pz)$_2$], 7.72 (t, J = 9.0 Hz, 2H, 5-H C_6H_4), 7.08 (d, J = 9.0 Hz, 4H, 4,6-H C_6H_4), 6.36/6.29 (s/s, 4H/4H, 4-H pz), 5.35 (s, 2H, 2-H C_6H_4), 2.68/2.60 (s/s, 12H/12H, 5-CH$_3$) 2.14/1.33 (s/s, 12H/12H, 3-CH$_3$). ^{13}C NMR (100.6 MHz, acetone-d_6): δ 153.4/151.7/146.1/145.4 (3,5-C pz, J_{C-Cd} = 6−10 Hz, J_{C-F} = 2 Hz), 135.2 (1,3-C C_6H_4), 130.1 (5-C C_6H_4), 129.0 (4,6-C C_6H_4), 126.6 (2-C C_6H_4), 108.3/106.9 (4-C pz), 68.1 [CH(pz)$_2$], 14.5/10.7 (3-CH$_3$), 10.3/9.9 (5-CH$_3$). ^{19}F NMR (376.2 MHz, acetone-d_6): δ −151 (s, 12F, BF_4^-), −223 (s, J_{F-Cd} = 30 Hz, 1F, Cd−F−Cd), ^{113}Cd NMR (88.8 MHz, acetone-d_6): δ 25.1 (d, J_{Cd-F} = 28 Hz). Anal. Calcd (found) for $C_{56}H_{68}B_3Cd_2N_{16}F_{13}$: C, 45.77 (45.74); H, 4.66 (4.40); N, 15.25 (15.05). MS ES(+) m/z (relative percent abundance) [assignment]: 1382 (12) $[Cd_2(\mathbf{L}_m^*)_2F(BF_4)_2]^+$, 648 (7) $[Cd_2(\mathbf{L}_m^*)_2F(BF_4)]^{2+}$, 614 (55) $[Cd\mathbf{L}_m^*F]^+$, 402 (100) $[Cd_2(\mathbf{L}_m^*)_2F]^{3+}$. HRMS ES$^+$ (m/z): $[Cd_2(\mathbf{L}_m^*)_2F(BF_4)_2]^+$ calcd for $[C_{56}H_{68}B_2Cd_2F_9N_{16}]^+$ 1383.3956; found 1383.4004.

*$[Mn_2(\mu\text{-}F)(\mu\text{-}\mathbf{L}_m^*)_2](ClO_4)_3$ (**7**).* Both $NaBF_4$ (0.028 g, 0.257 mmol) and $Mn(ClO_4)_2{\cdot}6H_2O$ (0.186 g, 0.514 mmol) were dissolved in THF (4 mL). Water (500 μL) was added to the mixture of the metal salts to

dx.doi.org/10.1021/ic301757g | Inorg. Chem. 2012, 51, 11820−11836

completely dissolve the $NaBF_4$. A THF (7 mL) solution of $\mathbf{L}_m$* (0.248 g, 0.514 mmol) was transferred by cannula into the metal salt solution. The reaction mixture was stirred for 5 h, after which time the solvents were removed by rotary evaporation. The white solid was washed with H_2O (20 mL) and dried under a vacuum overnight, affording 0.274 g of the crude product (77%). Single crystals suitable for X-ray studies were grown by the vapor diffusion of Et_2O into 1 mL of an acetonitrile solution of **7** (40 mg/mL). Anal. Calcd (found) for $C_{56}H_{68}Cl_3Mn_2N_{16}FO_{12}$: C, 48.30 (48.33); H, 4.92 (4.65); N, 16.09 (16.19). MS ESI(+) *m*/*z* (relative percent abundance) [assignment]: 1291 (5) $[Mn_2(\mathbf{L}_m*)_2F(ClO_4)_2]^+$, 596 (50) $[Mn_2(\mathbf{L}_m*)_2F(ClO_4)]^{2+}$, 556 (12) $[Mn\mathbf{L}_m*F]^+$, 483 (93) $[\mathbf{L}_m* + H]^+$, 364 (100) $[Mn_2(\mathbf{L}_m*)_2F]^{3+}$.

Crystallographic Studies. X-ray diffraction intensity data for compounds **1**–**6** were measured on a Bruker SMART APEX CCD-based diffractometer (Mo Kα radiation, λ = 0.71073 Å).[13] Raw area detector data frame processing was performed with the SAINT+ and SADABS programs.[13] Final unit cell parameters were determined by least-squares refinement of large sets of strong reflections taken from each data set. Direct-methods structure solution, difference Fourier calculations, and full-matrix least-squares refinement against F^2 were performed with SHELXTL.[14] Non-hydrogen atoms were refined with anisotropic displacement parameters, the exception being disordered species. The hydrogen atoms were placed in geometrically idealized positions and included as riding atoms. Details on data collection are given in Table 1, and details on the solution are provided in the Supporting Information.

RESULTS

Synthesis of $\mathbf{L}_m$*. The ligand was prepared by the cobalt(II)-catalyzed Peterson rearrangement[15] between isophthalaldehyde and $SO(3,5\text{-}Me_2pz)_2$, according to Scheme 2.

Scheme 2

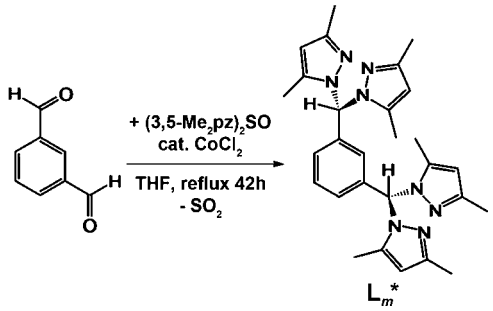

$SO(3,5\text{-}Me_2pz)_2$ was synthesized in situ from sodium pyrazolate and thionyl chloride. To achieve high yields (81%), the reaction time was increased (42 h) compared to that used in the preparation of $\mathbf{L}_m$ (24 h).[6a]

Syntheses of the Metallacycles. Compounds **1**–**6** were prepared by mixing separate THF solutions of $\mathbf{L}_m$* and $M(BF_4)_2{\cdot}xH_2O$ (M = Fe^{2+}, Co^{2+}, Ni^{2+}, Cd^{2+} x = 6; Cu^{2+} x = 3; Zn^{2+} x = 5) as shown in the equation

$$2M(BF_4)_2 + 2\mathbf{L}_m* \xrightarrow{THF} [M_2(\mu\text{-}F)(\mu\text{-}\mathbf{L}_m*)_2](BF_4)_3 + BF_3$$

where M = Fe^{2+} (**1**), Co^{2+} (**2**), Ni^{2+} (**3**), Cu^{2+} (**4**), Zn^{2+} (**5**), Cd^{2+} (**6**).

Compound **7** was isolated from the reaction of $Mn(ClO_4)_2{\cdot}6H_2O$ with $\mathbf{L}_m$* in the presence of $NaBF_4$, according to the equation

$$2Mn(ClO_4)_2 + NaBF_4 + 2\mathbf{L}_m* \xrightarrow{THF} [Mn_2(\mu\text{-}F)(\mu\text{-}\mathbf{L}_m*)_2](ClO_4)_3 + NaClO_4 + BF_3 \quad (7)$$

Solution Properties. A variety of NMR experiments (^1H, ^{13}C, and ^{19}F, as well as ^{113}Cd for **6**) were employed to study the solution behavior of the diamagnetic zinc(II) and cadmium(II) metallacycles. The ^1H NMR spectra of **5** and **6** (Figure 2) show one set of resonances for each type of hydrogen atoms in the *m*-phenylene spacers and the $-CH(3,5\text{-}Me_2pz)_2$ methine hydrogen atoms. In contrast, each type of hydrogen atom on the pyrazolyl rings exhibits two equal-intensity resonances, indicating two sets of nonequivalent pyrazolyl rings. Interestingly, the resonances for the *a**,*c**-methyl groups are at 2.55, 2.37, 1.68, and 0.73 ppm for **5**, and at 2.68, 2.60, 2.14, and 1.33 ppm for **6**, showing that one resonance in the second set for both compounds is highly shielded.

The assignments of the ^{13}C NMR signals in the spectra of **5** and **6** were made based on the heteronuclear single-quantum coherence (HSQC) spectra of the compounds. As observed in the ^1H NMR spectra, there is one set of resonances for each carbon atom type of the linking groups, but those on the pyrazolyl rings each show two. For the *a**,*c**-methyl group carbon atoms on the pyrazolyl rings (16.9, 11.5, 11.1, and 11.0 ppm for **5**; 14.5, 10.7, 10.3, and 9.9 ppm for **6**), again one of the resonances, this time for the first pair, is more shielded than expected (11.1 for **5**; 10.7 for **6**). The HSQC spectra show that these unusually shielded resonances correlate with the more shielded resonances in the ^1H spectra. The four distinct *a*- and *c*-pyrazolyl ring carbon resonances are at 154.6, 152.1, 146.0, and 145.9 ppm for **5** and at 153.4, 151.7, 146.1, and 145.4 ppm

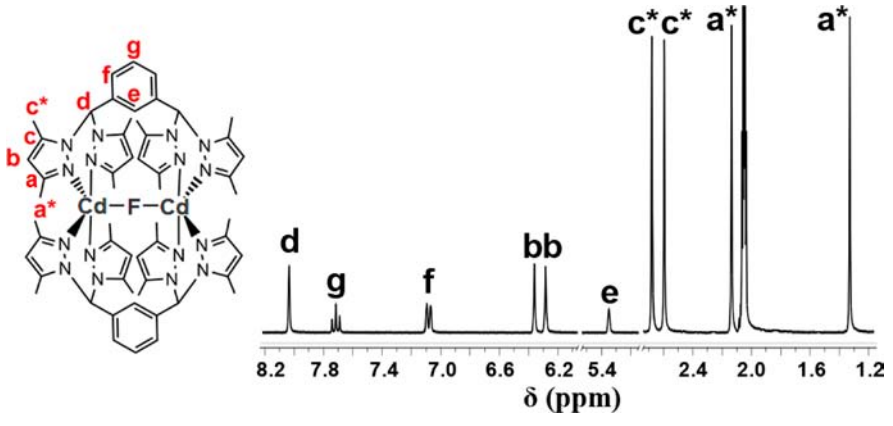

Figure 2. ^1H NMR spectrum of $[Cd_2(\mu\text{-}F)(\mu\text{-}\mathbf{L}_m*)_2](BF_4)_3$ (**6**).

dx.doi.org/10.1021/ic301757g | *Inorg. Chem.* 2012, 51, 11820–11836

for **6**. Cadmium satellites were observed with these resonances where J_{C-Cd} varies between 6 and 10 Hz (Figure 3). The resonance at 145.4 ppm was a doublet because of coupling with the bridging fluorine, with J_{C-F} = 2 Hz.

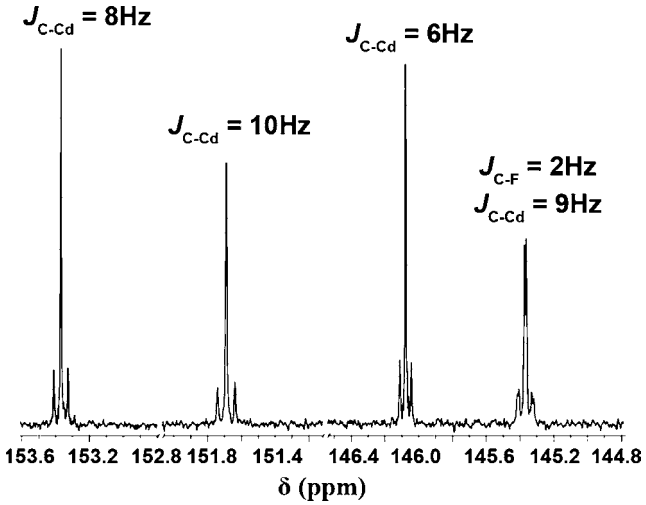

Figure 3. *a*- and *c*-pyrazolyl ring carbon resonances in the ^{13}C NMR spectrum of $[Cd_2(\mu\text{-}F)(\mu\text{-}\mathbf{L}_m\text{*})_2](BF_4)_3$.

The ^{19}F NMR spectra of both compounds show a resonance at −151.4 ppm, assigned to the BF_4^- anions. The smaller resonance at −151.3 can be associated with the isotopic distribution of boron. The bridging fluoride gives rise to a resonance at −173 ppm for compound **5** and at −224 ppm for compound **6**. The signal of the bridging fluoride in **6** is a singlet with $^{111/113}Cd$ satellites, the *J* value being 30 Hz (Figure 4). Similarly, the ^{113}Cd NMR spectrum of **6** shows a doublet resonance split by a similar magnitude of coupling from the bridging fluoride.

All of these results indicate that the dinuclear structures shown in the solid state (vide infra) are retained in acetonitrile and acetone solution for **5** and **6**, respectively. Consideration of the solid-state structures leads to the prediction that, if the same structures are present in solution, then two pairs of resonances

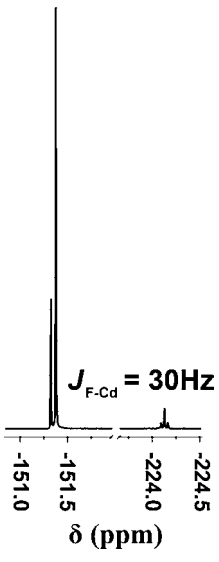

Figure 4. ^{19}F NMR spectrum of $[Cd_2(\mu\text{-}F)(\mu\text{-}\mathbf{L}_m\text{*})_2](BF_4)_3$.

should be observed for each hydrogen and carbon of the pyrazolyl rings, one set for those oriented along the M−F−M axis (equatorial) and another set for those perpendicular to it (axial), as is reported above. In contrast, each type of hydrogen and carbon atom in the *m*-phenylene spacers and the $-CH(pz)_2$ methine group should be equivalent, again as observed. Importantly, the bridging fluoride ligand gives rise to a resonance in the ^{19}F NMR spectra of both complexes, a resonance for **6** that shows appropriate satellites for coupling to cadmium, with the reverse coupling to a single fluoride nucleus observed in the ^{113}Cd NMR spectrum. Coupling to both fluorine and cadmium is also observed in some of the ^{13}C resonances.

Finally, the hydrodynamic radius of **5** was measured from the diffusion coefficient of the complex in solution as determined by pulsed field-gradient spin−echo NMR (PFGSE-NMR) spectroscopy. The radius determined from this experiment is 9.2 Å, whereas the hypothetical radius, calculated from the X-ray crystal structure of the dinuclear zinc(II) compound, is 8.4 Å. The accuracy of this method is believed to be in the 20% range.

Mass Spectrometry. Positive-ion electrospray mass spectra (ESI^+-MS) of all seven complexes are similar. Clusters, such as $[M_2(\mathbf{L}_m\text{*})_2F(BF_4)_2]^+$ and $[M_2(\mathbf{L}_m\text{*})_2F]^{3+}$, where M = Fe(II), Co(II), Ni(II), Cu(II), Zn(II), and Cd(II), are observed in all spectra that correspond to the fluoride-bridged metallacycles. The ESI^+-MS spectra of **7** shows similar peaks with the corresponding ClO_4^- counterions. For **1**−**3**, **6**, and **7**, the base peak in the spectrum is $[M_2(\mathbf{L}_m\text{*})_2F]^{3+}$; for compounds **4** and **5**, it also has relatively high intensity. A set of peaks for $[M_2(\mathbf{L}_m\text{*})_2F(A)]^{2+}$ (A = BF_4^- for **1**−**4** and **6** or ClO_4^- for **7**) is observed in all spectra except for **5**. Fragments of the metallacycles, like $[ML_m\text{*}F]^+$, were also detected with high intensities. In the ESI^+-MS spectra of compounds **1**−**7**, no polymeric species were observed, indicating that the metallacycles are highly stable even in the gas phase. These observations are in good agreement with the structures determined in the solid state and for **5** and **6** in solution.

Solid-State Structures. Figure 5 shows the structure of the dinuclear fluoride-bridged cation for compound **1**, $[Fe_2(\mu\text{-}F)(\mu\text{-}\mathbf{L}_m\text{*})_2](BF_4)_3$, where the numbering scheme is correct for all of the structures of **1**−**6**, with the exception of the low-temperature structure of the copper(II) complex **4**, vide infra. As shown in Table 2 and Table S1, which contains selected bond lengths, the structures of the cationic units are very similar.

The structures of **1**−**6** are centrosymmetric (center of symmetry at fluoride), except for the low-temperature structure of **4**, vide infra. The geometry around the metal centers is a distorted trigonal bipyramid; the fluoride (F1) and N11, N31 are equatorial, and N21 and N41 are axial. The equatorial angles are distorted from the ideal values (120°) (for example, in **1**, N−M−F = 135.94°, 132.32°; N−M−N = 91.71°), whereas the axial−axial angle is almost ideal (180°) (e.g., in **1**, N−M−N = 177.12°). In addition, the trigonal bipyramidal geometry is indicated by the τ_5 values, a general descriptor of five-coordinate systems[16] that is calculated according to the equation $\tau_5 = (\beta - \alpha)/60°$, where α and β are the two largest angles measured around the metal centers. A perfect square pyramid is given by a τ_5 value of 0, and a perfect trigonal bipyramid has a value of 1. The τ_5 values for **1**−**7** are summarized in Table 2, and in all cases, they support the distorted trigonal bipyramidal geometry around the metal

dx.doi.org/10.1021/ic301757g | *Inorg. Chem.* 2012, 51, 11820−11836

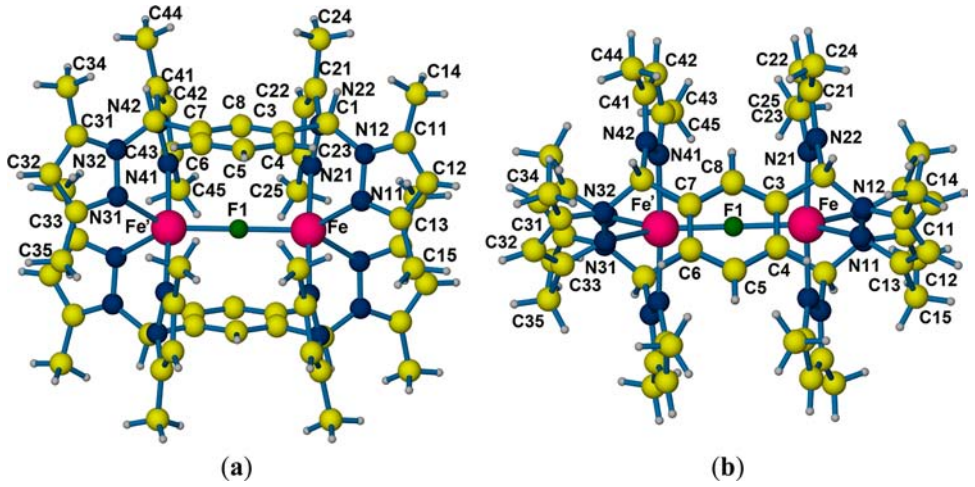

Figure 5. Structure of the cation in $[Fe_2(\mu\text{-}F)(\mu\text{-}L_m^*)_2](BF_4)_3$ (**1**): (a) front view, (b) top view.

Table 2. Important Structural Parameters for $[Fe_2(\mu\text{-}F)(\mu\text{-}L_m^*)_2](BF_4)_3$ (1), $[Co_2(\mu\text{-}F)(\mu\text{-}L_m^*)_2](BF_4)_3$ (2), $[Ni_2(\mu\text{-}F)(\mu\text{-}L_m^*)_2](BF_4)_3\cdot 2H_2O$ ($3\cdot 2H_2O$), $[Cu_2(\mu\text{-}F)(\mu\text{-}L_m^*)_2](BF_4)_3$ (4), $[Zn_2(\mu\text{-}F)(\mu\text{-}L_m^*)_2](BF_4)_3\cdot 2H_2O$ ($5\cdot 2H_2O$), $[Cd_2(\mu\text{-}F)(\mu\text{-}L_m^*)_2](BF_4)_3\cdot 2CH_3CN$ ($6\cdot 2CH_3CN$), and $[Mn_2(\mu\text{-}F)(\mu\text{-}L_m^*)_2](ClO_4)_3\cdot 2CH_3CN$ ($7\cdot 2CH_3CN$)

complex	temp (K)	metal centers	M−F−M angle (deg)	M−F distance (Å)	$dL_m^*(M-F) - dL_m(M-F)$[a]	predicted M−F distance[d] (Å)	average M−N distance (Å)	τ_5	M···M distance (Å)
1	296	Fe(1)−Fe(1′)	180.00	2.0231(4)	+0.079/+0.048[b]	2.00	2.149	0.69	4.05
2	296	Co(1)−Co(1′)	180.00	2.0626(4)	+0.111/+0.085[b]	1.96	2.099	0.74	4.13
$3\cdot 2H_2O$	150	Ni(1)−Ni(1′)	180.00	2.0603(3)	–	1.92	2.057	0.71	4.12
4	296	Cu(1)−Cu(1′)	180.00	2.0631(8)	+0.113/+0.080[b]	1.94	2.072	0.72	4.13
4	100	Cu(1A)−Cu(2A)	175.60(14)	2.025(3)/ 2.038(3)	+0.068/+0.081[c]	1.94	2.058/2.059	0.74/0.68	4.061
		Cu(1B)−Cu(2B)	176.10(16)	2.013(3)/ 2.048(3)	+0.056/+0.091[c]		2.058/2.057	0.67/0.75	4.082
		Cu(1C)−Cu(2C)	179.0(3)	2.027(5)/ 2.055(6)	+0.070/+0.098[c]		2.066/2.054	0.70/0.69	4.058
$5\cdot 2H_2O$	150	Zn(1)−Zn(1′)	180.00	2.0456(2)	+0.107/+0.040[b]	1.97	2.113	0.77	4.09
$6\cdot 2CH_3CN$	100	Cd(1)−Cd(1′)	180.00	2.1507(2)	–	2.16	2.307	0.78	4.30
$7\cdot 2CH_3CN$	100	Mn(1)−Mn(1′)	180.00	2.0293(3)	–	2.04	2.235	0.70	4.06
		Mn(2)−Mn(2′)	180.00	2.0669(3)			2.219	0.71	4.13

[a]Difference between the M−F distance in the L_m^* compounds $[dL_m^*(M-F)]$ and the M−F distance in the L_m compounds $[dL_m(M-F)]$; see ref 6b for $dL_m(M-F)$. [b]Two different values of $dL_m^*(M-F) - dL_m(M-F)$, because the L_m fluoride-bridged compounds have two crystallographically independent cations in the unit cell. [c]Average of the $dL_m^*(M-F) - dL_m(M-F)$ values. [d]Reference 17.

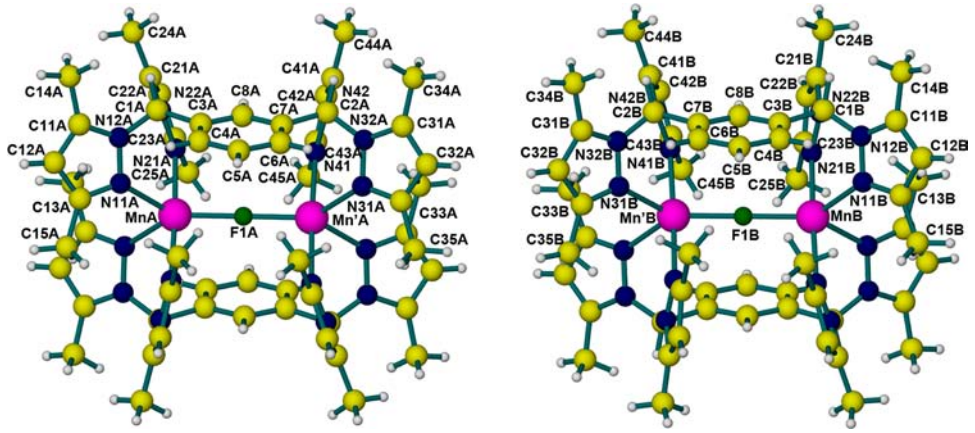

Figure 6. Structure of the two independent cationic units of $[Mn_2(\mu\text{-}F)(\mu\text{-}L_m^*)_2](ClO_4)_3$ (**7**).

centers. The axial M−N bond lengths are shorter than the equatorial M−N bond lengths in the range of 0.01−0.05 Å in all complexes except for the copper(II) complex **4**, an arrangement in disagreement with electrostatic predictions.[18]

dx.doi.org/10.1021/ic301757g | Inorg. Chem. 2012, 51, 11820−11836

The compression of the axial bonds is very large in **4**, where the axial bond lengths are 0.175 Å shorter.

In the structure of $[Mn_2(\mu\text{-}F)(\mu\text{-}L_m^*)_2](ClO_4)_3$ (**7**) there are two independent cationic units (see Figure 6). Both cations reside on crystallographic inversion centers; the overall structures are similar to each other and to those of compounds **1**−**6**. An unusual result observed for compound **7** is that the Mn−F bond length in one of the independent cations is smaller (2.029 Å) than that in the other (2.067 Å). As expected, the cation with the shorter M−F bond length shows longer Mn−N bond lengths than the other cation by an average of 0.016 Å.

Phase Change of $[Cu_2(\mu\text{-}F)(\mu\text{-}L_m^*)_2](BF_4)_3$ (4). Lowering the temperature of crystals of compounds **1**, **2**, and **4** leads to a structural phase transition. Only in the case of **4**, where the phase transition takes place reversibly at 250 K (T_{trans}), could the lower-temperature structure be properly determined. The phase transition involves partial ordering (cooling) or disordering (warming) of the tetrafluoroborate anions and shifts in cation geometries and positions (Figure 7). The cation

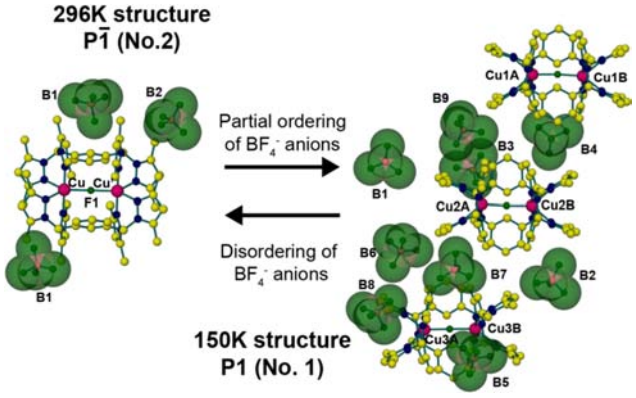

Figure 7. Phase change of $[Cu_2(\mu\text{-}F)(\mu\text{-}L_m^*)_2](BF_4)_3$ (**4**). Hydrogen atoms and disordered BF_4^- anions were omitted for clarity (disordered BF_4^- species: B1 and B2 in the high-temperature structure; B2 and B4−B8 in the low-temperature structure).

geometry changes and the displacements of the cations within the unit cell are likely a response to the ordering movement of the anions below the transition temperature. Upon cooling below T_{trans}, the (half of) one unique, centrosymmetric cation in the asymmetric unit is transformed into three unique, noncentrosymmetric cations. A good indicator of the distortion of the cation geometry in the low-temperature form is given by the continuous symmetry measure (CSM S' value),[19] calculated by PLATON.[20] This parameter gives the measure of deviation from a given point symmetry, with a CSM value of 0 corresponding to ideal point symmetry and higher values representing increasingly larger departures from ideal symmetry. In the high-temperature form, the single cation has crystallographically imposed C_i point symmetry (CSM ≡ 0). The CSM values for the three low-temperature cations are A = 1.0, B = 1.0, and C = 0.1. The large deviations from inversion symmetry for cations A and B can be seen most obviously in their bent Cu−F−Cu angles of 175.6° and 176.1°, respectively. For cation C, this angle is 179.0°. The changes in crystal packing are depicted in the Supporting Information. Figure S3 (Supporting Information) shows both forms viewed along corresponding directions ($[100]_{HT}$ = $[1\bar{1}\bar{1}]_{LT}$), showing misalignment of the cations and anions in the low-temperature form in projection along this direction. Figure S4 (Supporting Information) shows both structures viewed along the equivalent directions $[010]_{HT}$ and $[100]_{LT}$. Figure S5 (Supporting Information) shows the equivalent views $[001]_{HT}$ and $[\bar{2}2\bar{1}]_{LT}$.

Magnetic Properties and EPR Spectra. The exchange coupling between two ions with spin $S_1 = S_2$ gives rise to a series of coupled spin states characterized by the total spin quantum number S ranging from 0 to $2S_1$. The Heisenberg−Dirac−Van Vleck Hamiltonian in the form

$$\hat{\mathbf{H}} = -J\hat{\mathbf{S}}_1\hat{\mathbf{S}}_2 \tag{1}$$

has typically been applied to interpret the magnetic properties of the dinuclear complexes. The energies of the S levels are

$$E(S) = -(J/2)[S(S+1) - 2S_1(S_1+1)] \tag{2}$$

If the exchange coupling is sufficiently large, the S levels are "pure", and both the EPR and magnetic problems can be handled using the coupled-spin representation (often called the "giant-spin" approximation), in which a separate spin Hamiltonian is defined for each of the different coupled S states

$$\hat{\mathbf{H}}_S = \mu_B\mathbf{B}\cdot\{\mathbf{g}_S\}\cdot\hat{\mathbf{S}} + D_S[\hat{\mathbf{S}}_z^{\,2} - S(S+1)/3] + E_S(\hat{\mathbf{S}}_x^{\,2} - \hat{\mathbf{S}}_y^{\,2}) \tag{3}$$

The zero-field splitting parameters D_S and E_S are different in each coupled spin state, and they contain contributions due to the zero-field splitting on individual ions with $S_1 > {}^1/_2$, D_1, D_2 and E_1, E_2, as well as a contributions D_{12} and E_{12} due to the anisotropic interactions between the metal ions[21,22]

$$D_S = \alpha_S D_{12} + \beta_S(D_1 + D_2)$$
$$E_S = \alpha_S E_{12} + \beta_S(E_1 + E_2) \tag{4}$$

where

$$\alpha_S = [S(S+1) + 2S_1(S_1+1) + 2S_2(S_2+1)]/[2(2S-1)(2S+3)]$$
$$\beta_S = [3S(S+1) - 2S_1(S_1+1) - 2S_2(S_2+1) - 3]/[2(2S-1)(2S+3)] \tag{5}$$

In the present case, large zero-field splitting, comparable to the exchange coupling, is expected for the iron(II), cobalt(II), and nickel(II) complexes, causing the S levels to mix. For this reason, the above treatment is not adequate, and the spin Hamiltonian needs to be expressed in terms of the spin operators of the individual ions

$$\begin{aligned}\hat{\mathbf{H}} = {} & -J\hat{\mathbf{S}}_1\hat{\mathbf{S}}_2 \\ & + D_{12}(\hat{\mathbf{S}}_{z1}\hat{\mathbf{S}}_{z2} - \hat{\mathbf{S}}_1\cdot\hat{\mathbf{S}}_2/3) + E_{12}(\hat{\mathbf{S}}_{x1}\hat{\mathbf{S}}_{x2} - \hat{\mathbf{S}}_{y1}\hat{\mathbf{S}}_{y2}) \\ & + \mu_B B\{\mathbf{g}_1\}\hat{\mathbf{S}}_1 + D_1[\hat{\mathbf{S}}_{z1}^{\,2} - S_1(S_1+1)/3] \\ & + E_1(\hat{\mathbf{S}}_{x1}^{\,2} - \hat{\mathbf{S}}_{y1}^{\,2}) + \mu_B B\{\mathbf{g}_2\}\hat{\mathbf{S}}_2 \\ & + D_2[\hat{\mathbf{S}}_{z2}^{\,2} - S_2(S_2+1)/3] + E_2(\hat{\mathbf{S}}_{x2}^{\,2} - \hat{\mathbf{S}}_{y2}^{\,2})\end{aligned} \tag{6}$$

In the centrosymmetric complexes studied here, $D_1 = D_2$, $E_1 = E_2$, and the $\{g\}$ tensors of the two ions are equal and coaxial. For that reason, the $\{g\}$ tensors in each coupled state must be equal to each other and equal to $\{g\}$ on individual ions. Both the dipole−dipole and anisotropic exchange interactions

contribute to D_{12} and E_{12}. The spin Hamiltonian in eq 6 can be used to explain both the magnetic properties and the EPR spectra. Its application is much more difficult than using the giant-spin method. For example, in the case of an Fe(II) dinuclear system, spin Hamiltonian matrices of dimension 25 × 25 have to be diagonalized, whereas the coupled representation method would use 3 × 3, 5 × 5, 7 × 7, and 9 × 9 matrices for total spin states 1, 2, 3, and 4, respectively.

Because no analytical formulas are available for the energy levels of the manganese(II), iron(II), cobalt(II), and nickel(II) dinuclear compounds if the zero-field splitting on individual metal ions and the Zeeman term need to be included, their magnetic susceptibility, χ_d, has to be evaluated from the basic relation

$$\chi_d = -\frac{N}{B}\frac{\sum_i \frac{\partial E_i}{\partial B}\exp(-E_i/kT)}{\sum_i \exp(-E_i/kT)} + 2\text{TIP} \quad (7)$$

where the summation runs over all states in the system. The energies were found by diagonalizing the matrix of the spin Hamiltonian (eq 6) The derivatives $\delta E_i/\delta B$ were calculated numerically, by evaluating energies, E_i, 5 G below and 5 G above the magnetic field of the SQUID instrument (5000 G). As in other dinuclear complexes, a contribution to magnetic susceptibility due to mononuclear impurities was observed, which was taken into account by fitting experimental data to the expression

$$\chi = (1 - f)\chi_d + 2f\chi_m \quad (8)$$

where f is the fraction of a mononuclear impurity and χ_m is its molar magnetic susceptibility. For the Mn(II), Fe(II), Co(II), and Ni(II) compounds, χ_d was calculated from eq 7 and χ_m was expressed as

$$\chi_m = -\frac{N\mu_B g}{B}\frac{\sum_{M_S=-S}^{S} M_S \exp(-g\mu_B BM_S/kT)}{\sum_{M_S=-S}^{S} \exp(-g\mu_B BM_S/kT)} + \text{TIP} \quad (9)$$

In the much simpler case of the copper(II) complexes, where the giant-spin method and the spin Hamiltonian in eq 3 are applicable, χ_d was evaluated from the well-known Bleaney–Bowers expression[22]

$$\chi_d = \frac{N\mu_B{}^2 g^2}{3kT}\frac{6\exp(J/kT)}{1 + 3\exp(J/kT)} + 2\text{TIP} \quad (10)$$

and χ_m was calculated from Curie's law

$$\chi_m = (N\mu_B{}^2 g^2/3kT) \times 0.75 + \text{TIP} \quad (11)$$

Figure 8 shows the magnetic susceptibility for compounds **1**–**4** and **7**, and Table 3 lists the spin Hamiltonian parameters. All of the compounds are antiferromagnetically coupled, although the magnitude of the coupling changes dramatically. An interesting feature of the susceptibilities of the iron(II), cobalt(II), and nickel(II) complexes is that they do not drop to zero at the lowest temperatures (even if the monomer contribution is subtracted), a result caused by very large zero-field splitting in the excited paramagnetic states. The magnetic susceptibility of nickel(II) complex **3** calculated with and without the D_1 term is shown in the Supporting Information (Figure S6). The susceptibility of the manganese(II) complex does not reach zero at 1.8 K because of the small J value. The magnitude of the antiferromagnetic coupling increases across

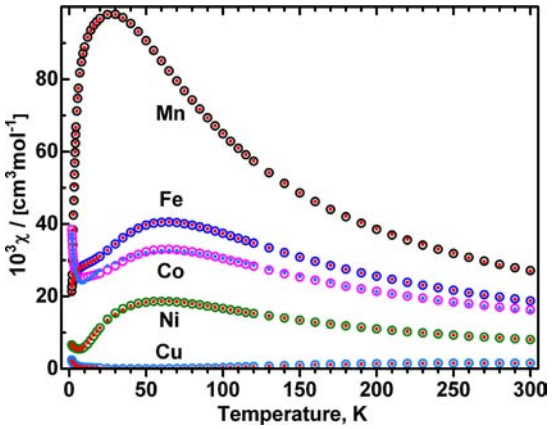

Figure 8. Magnetic susceptibility of (top to bottom) $[Mn_2(\mu\text{-F})(\mu\text{-}\mathbf{L}_m\text{*})_2](ClO_4)_3\cdot 2CH_3CN$ (**7**·2CH_3CN), $[Fe_2(\mu\text{-F})(\mu\text{-}\mathbf{L}_m\text{*})_2](BF_4)_3$ (**1**), $[Co_2(\mu\text{-F})(\mu\text{-}\mathbf{L}_m\text{*})_2](BF_4)_3$ (**2**), $[Ni_2(\mu\text{-F})(\mu\text{-}\mathbf{L}_m\text{*})_2](BF_4)_3\cdot 2H_2O$ (**3**·2H_2O), and $[Cu_2(\mu\text{-F})(\mu\text{-}\mathbf{L}_m\text{*})_2](BF_4)_3$ (**4**). Open circles, experimental data; solid dots, calculated values. The g, J, and D_1 values for the Fe(II), Co(II), and Ni(II) complexes were determined from the magnetic data (Table 3), whereas for Mn(II), the EPR values of $D_1 = -0.3254$ cm^{-1}, $E_1 = -0.0153$ cm^{-1}, $D_{12} = 0.0302$ cm^{-1}, and $E_{12} = 0$ were fixed, and g and J were fitted. See Figure 11 for an expansion and details on $[Cu_2(\mu\text{-F})(\mu\text{-}\mathbf{L}_m\text{*})_2](BF_4)_3$.

the periodic table from left to right, with the value for the copper(II) complex **4** dramatically larger than those for the other metals, −322 cm^{-1}.

*Magnetic Properties and EPR Spectra of $[Mn_2(\mu\text{-F})(\mu\text{-}\mathbf{L}_m\text{*})_2](ClO_4)_3\cdot 2CH_3CN$ (**7**).* The exchange integral was determined by fitting the magnetic susceptibility using eqs 7–9. The zero-field splitting (zfs) parameters were fixed at the values found from EPR (see below), and only J and g were allowed to vary. Small differences between the g values from EPR and from magnetic susceptibility (Table 3) are often observed. The temperature-independent paramagnetism (TIP) was assumed to be 0, and the fraction of mononuclear impurities of 0.2% was obtained. The complex exhibits well-resolved high-field EPR spectra in which the positions of the resonance lines that can be assigned to the $S = 1$ and $S = 2$ states are almost temperature-independent over the temperature range of 3–50 K. Although the giant-spin model is not strictly applicable, it is still useful to classify the EPR transitions according to the total spin state in which they occur. Comparison of calculations using the spin Hamiltonian in eq 3 versus that in eq 6 indicates that, with a J value of ca. −7 cm^{-1} and D_1 on individual manganese(II) ions of approximately −0.3 cm^{-1}, the spin state mixing affects the $S = 1$ state of the dinuclear system only marginally, whereas its effect on the $S = 2$ state is significant. The spin state mixing causes a shift of the $M_S = 0$ level of $S = 2$, so that the energies of the M_S levels no longer follow the $E(M_S) = D_S M_S{}^2$ dependence. However, the energy difference between levels $M_S = \pm 1$ and $M_S = \pm 2$ remains largely unaffected. In an $S = 2$ state, there are four "allowed" transitions at each orientation of the magnetic field. The outer of the four resonances at Z orientation (labeled 2z in Figure 9), which correspond to transitions $(-2) \leftrightarrow (-1)$ and $(2) \leftrightarrow (1)$ could therefore be used to determine the $D_{S=2}$ magnitude of 0.341 cm^{-1}. The $S = 1$ spectrum can be very well simulated at each microwave frequency according to the giant-spin (i.e., coupled-representation) model (eq 3) with $S = 1$, $g_x = g_y = 2.005$, $g_z = 2.000$, $D_{S=1} = 2.187$ cm^{-1}, and $E_{S=1} = 0.0935$ cm^{-1}. The intensity of the low-field $\Delta M_S = 1$ resonance (1z at 4.9 T in Figure 9) is suppressed when the temperature is

dx.doi.org/10.1021/ic301757g | *Inorg. Chem.* 2012, 51, 11820–11836

Table 3. Experimental Spin Hamiltonian Parameters and Results of DFT Calculations

	1 (Fe)	**2** (Co)	**3**·2H_2O (Ni)	**7**·2CH_3CN (Mn)	**4** (Cu)
g_{avg} (magnetic)	2.11	2.26	2.31	2.02	2.22
g_x, g_y, g_z (EPR)	2.26, 2.29, 1.99	–	–	2.00, 2.00, 2.00	2.15, 2.33, 2.01
$-J$ (cm^{-1}) (exp)	16.3(3)[a]	24.1(5)[a]	39.0(1)[a]	6.7(2)[a]	322(5)[a]
$-J$ (cm^{-1}) (DFT)	28	–	55	12 long, 14 short[c]	380
D_1 (cm^{-1})	−10.0(3),[a] −9.89(2)[b]	20(2)[a]	36(1)[a]	−0.325(2)[b]	0.173(2)[b,d]
E_1 (cm^{-1})	0	0	0	−0.0153(2)[b]	0.089(2)[b,d]

[a]Parameters from magnetic susceptibility. [b]Parameters from EPR. [c]Data for two molecules with slightly different Mn−F bond lengths. [d]D and E refer to the coupled-spin Hamiltonian (eq 3); other D and E values are for the spin Hamiltonian (eq 6).

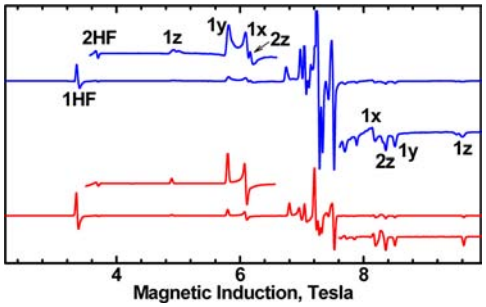

Figure 9. EPR spectra of $[Mn_2(\mu\text{-F})(\mu\text{-}\mathbf{L}_m\text{*})_2](ClO_4)_3$·2$CH_3CN$. Top (blue): experimental spectrum, recorded at 10 K with ν = 203.2 GHz. Bottom (red): simulated spectrum obtained using the Hamiltonian in eq 6 with $g_x = g_y = g_z = 2.00$, $D_1 = -0.3254$ cm^{-1}, $E_1 = -0.0153$ cm^{-1}, $J = -6.7$ cm^{-1}, $D_{12} = 0.0302$ cm^{-1}, and $E_{12} = 0$. Note that the doubling of some resonances in the experimental spectrum (at 4.8 and at 9.6 T) is presumably due to two dinuclear species with slightly different Mn−F bond lengths (see the Crystallographic Studies section). The numbers 1 and 2 indicate the spin states in which transitions occur; letters x, y, and z indicate the molecular orientations. HF means the half-field, "forbidden transition", $\Delta M_S = 2$. The HF transition in $S = 1$ is at a lower magnetic field than that in $S = 2$ because of much larger zfs parameters in the former.

lowered, whereas the intensity of the high-field 1z resonance (9.6 T) increases. These trends confirm that $D_{S=1}$ is positive.[23] $D_{S=2}$ is also positive (high-field 2z line becomes stronger with decreasing temperature, and the low-field 2z line disappears). Determination of D in both $S = 1$ and $S = 2$ states allows calculation of $D_1 = -0.320$ cm^{-1} and $D_{12} = 0.036$ cm^{-1} (eqs 4 and 5). This analysis assumes that the coordinate systems for D_1 and D_{12} are parallel (or exactly orthogonal), which is likely to be obeyed by our molecules. Using the software package ORCA,[24] we have attempted the density functional theory (DFT) calculation using the TZVPP basis set for manganese(II) and all coordinated atoms and SVP for other atoms, combined with the B3LYP functional, of D_1 on individual ions. The calculations were performed on a fragment containing one metal ion with its ligands and the bridging atom. In the case of **7**·2CH_3CN, the DFT method gave $D_1 = -0.06$ cm^{-1} with the z axis of the zfs (zero-field splitting) tensor along the bipyramid vertical axis. It is known that DFT does not produce reliable D_1 values. In the experience of some of us,[25] the unrestricted Hartree−Fock (UHF) calculations of D_1 tend to be better (although this has been criticized). In the present case, we obtained from UHF (available within ORCA as well) $D_1 = -0.10$ cm^{-1}, still much less than the experimental value. In general, the orientation of the zero-field splitting tensor is calculated more properly than its magnitude. With the Mn···Mn distance of 4.1 Å, the dipolar contribution to D_{12} of eq 6 is $D_{12}^{dipolar} = -3\mu_B^2 g^2/r_{Mn-Mn}^3 = -0.075$ cm^{-1}. This value should be considered as an upper limit, because the formula takes no electron delocalization into account, and $E_{12}^{dipolar}$ is 0. The z component of the dipolar interaction lies along the Mn···Mn direction, whereas the z axis of D_1 is along the trigonal bipyramid axis, roughly perpendicular. Rotation of the dipolar interaction tensor into the D_1 system produces $D_{12}^{dipolar} = +0.037$ cm^{-1} and $E_{12}^{dipolar} = 0.037$ cm^{-1}. Thus, the dipolar part appears to account for the magnitude of D_{12} found above from the EPR spectra analysis.

The parameters above were used as seed values in a procedure fitting the dependence of the resonance fields versus frequency, which is explained in a more detailed way in the next section (for **1**). The spectrum in Figure 9 was simulated with the parameters refined in this way. The magnetic susceptibility in Figure 8 was calculated using the same zfs parameters.

Mantel et al.[26] used HF EPR to investigate some mononuclear trigonal bipyramidal manganese(II) complexes and observed negative D values (−0.3 cm^{-1}) in axially elongated molecules, whereas our manganese(II) complex is axially compressed. Their complexes, however, are too dissimilar from ours to make a direct comparison.

Magnetic Properties and EPR Spectra of $[Fe_2(\mu\text{-F})(\mu\text{-}\mathbf{L}_m\text{*})_2](BF_4)_3$ *(**1**).* The magnetic susceptibility of **1** could be very well reproduced using the spin Hamiltonian (eq 6) in which the anisotropic metal−metal interactions were neglected. The zero-field splitting in this dinuclear compound is expected to be dominated by the $D_1 = D_2$, $E_1 = E_2$ terms, which are typically very large in iron(II). Fitting with eqs 7−9 resulted in $J = -16.3$ cm^{-1} and $D_1 = -10.0$ cm^{-1}, which are similar to the values observed in the unsubstituted complex.[6] Similar J and D_1 values were also found in other dinuclear iron(II) complexes.[23] The fraction of mononuclear impurities was 0.04%, and TIP was 0. It is known that magnetic susceptibility fitting is often insensitive to the sign of D_1 on single metal ions, even in the mononuclear systems. Somewhat surprisingly, this insensitivity is not true in the present case, as no reasonable fit was possible with $D_1 > 0$. This result can be understood by inspection of the energy diagrams calculated for positive or negative $D_1 = D_2$ (see the Supporting Information).

With $D_1 = D_2 = -10$ cm^{-1} and $J = -16$ cm^{-1}, the lowest level of the dinuclear compound is $S = 0$, $M_S = 0$, followed by $S = 1$, $M_S = 0$ at 2.6 cm^{-1} above it and the $S = 1$, $M_S = \pm 1$ pair at 44.4 cm^{-1} above the ground level (Figure S7, Supporting Information). With D_1 positive, the $S = 1$, $M_S = \pm 1$ pair lies 13.8 cm^{-1} above the $S = 0$, $M_S = 0$ state, and the $S = 1$, $M_S = 0$ is 49.8 cm^{-1} above the diamagnetic ground level (Figure S8, Supporting Information). These two energy diagrams predict very different magnetic behavior with only the negative sign of D_1 fitting the data, thus clearly establishing the sign.

High-field EPR spectra of **1**, recorded with frequencies of 50−420 GHz, were very weak and noisy, yet they were well

dx.doi.org/10.1021/ic301757g | Inorg. Chem. 2012, 51, 11820−11836

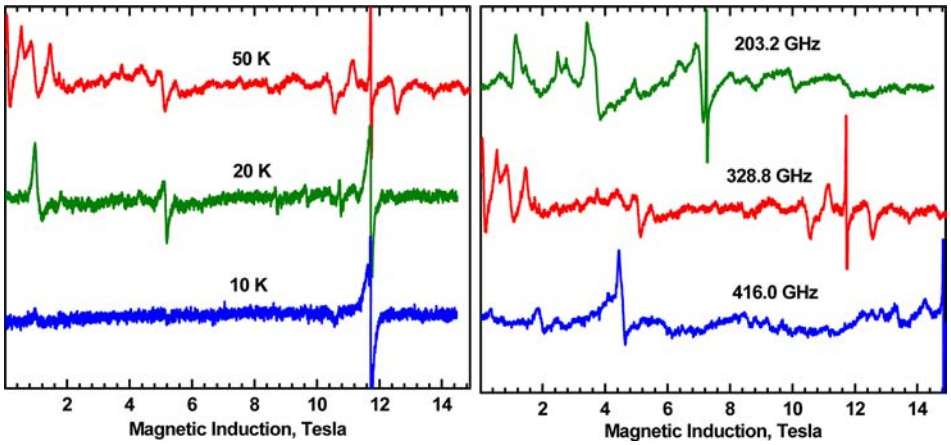

Figure 10. (Left) EPR spectra of $[Fe_2(\mu\text{-}F)(\mu\text{-}\mathbf{L}_m\text{*})_2](BF_4)_3$ (**1**) at the indicated temperatures and ν = 328.8 GHz. The sharp resonance at 11.74 T ($g \approx 2.003$) is a free-radical contamination. The spectrum intensity decreases with decreasing temperature, as expected for this antiferromagnetic iron(II) compound. (Right) EPR spectrum of **1** recorded at 50 K and the indicated microwave frequencies. Note that a resonance near zero magnetic field is observed at ν = 328.8 GHz.

reproducible and contained large numbers of resonance lines. Spectra shown in Figure 10 are presumably the first ever observed for an iron(II) dinuclear system in which the allowed transitions between states split by D are directly observed. X-band spectra of diferrous systems can sometimes be detected even at the X-band. In cases where E is small compared to D, the X-band-active transitions occur between levels such as M_S = 4 and M_S = −4, within an S = 4 state, which are split in zero magnetic field by $\sim E^2/D$ (second-order perturbation calculation). Being forbidden, ΔM_S = 8 transitions, they appear at very high effective g values and carry only limited information on the zero-field splitting.[27]

In the present case, the HF EPR spectra could be observed at temperatures as high as 120 K, had the best quality at about 50 K, and disappeared completely below 10 K, in agreement with the energy diagram derived for J = −16 cm^{-1} and D_1 = −10 cm^{-1}. When the giant-spin method is applied, D_1 = −10 cm^{-1} results in $D_{S=1}$ = +42 cm^{-1} in the triplet state (S = 1) of the dinuclear compound, $D_{S=2}$ = +4.28 cm^{-1} in the S = 2 state, and $D_{S=3}$ = −2 cm^{-1} in the S = 3 state. In the present case J is not large enough compared to D_1, and these relations are somewhat altered due to the spin state mixing: The distance between the M_S = 0 and M_S = ± 1 pair of the nominal triplet state is 41.77 cm^{-1} when calculated with the Hamiltonian in eq 6, instead of 42 cm^{-1}. These relatively small differences strongly affect the EPR spectra. With J and D_1 as determined from the magnetic susceptibility, a resonance at nearly zero magnetic field is expected at 328.8 GHz, and it is indeed observed (Figure 10; Figure S7, Supporting Information). This resonance corresponds to an allowed transition from M_S = −2 to M_S = −1 within the nominal S = 3 state. A method frequently used in this laboratory was employed to determine the spin Hamiltonian parameters. Instead of attempting to simulate the powder EPR spectra, which is extremely time-consuming (the spin Hamiltonian matrix has a size of 25 × 25, and a powder simulation requires calculation of many thousands of single-crystal-type spectra), the frequency dependencies of some well-defined resonances were fitted. In the present case, the best defined canonical resonances (at x, y, and z orientations) were observed in the 295−334 GHz range, and mainly those were used in the fitting procedure (see Figure S9, Supporting Information).

The fitting did not change the D_1 and J values found from the magnetic susceptibility much. Values of g_x = 2.26, g_y = 2.29, g_z = 1.99, J = −16.0 cm^{-1}, D_1 = −9.89 cm^{-1}, and D_{12} = −0.065 cm^{-1} were obtained. DFT calculations, such as those for the manganese(II) complex above, resulted in D_1 = −3.6 cm^{-1} with the largest component of the zfs tensor along the Fe−F axis, and therefore, there was no need for rotating the D_{12}^{dipolar} tensor. D_{12}^{dipolar} calculated from the point-dipole formula is −0.086 cm^{-1} and compares well to D_{12} above. The UHF calculations ended with error (crashing in the phase of calculating D). The most interesting result here is that D_1 on the iron(II) ions is negative and that the largest zfs component is directed toward the bridge. Negative D_1 values have been reported in strongly elongated trigonal pyramidal iron(II) compounds.[28] Unfortunately, no direction of zfs has been reported, but it is likely to be along the pyramid axis. Those complexes are actually trigonal, having three N atoms in the equatorial plane. Indeed, it is the axially elongated iron(II) trigonal bipyramid that is supposed to exhibit negative D_1.[29] However, the coordination-sphere symmetry in our compounds is not perfectly trigonal, but rather resembles C_{2v}, which is responsible for the negative D_1 value and its orientation, as confirmed by the DFT results.

*Magnetic Properties of $[Co_2(\mu\text{-}F)(\mu\text{-}\mathbf{L}_m\text{*})_2](BF_4)_3$ (**2**) and $[Ni_2(\mu\text{-}F)(\mu\text{-}\mathbf{L}_m\text{*})_2](BF_4)_3\cdot 2H_2O$ (**3**·2H$_2$O).* No EPR spectra were observed at any temperature and frequency. Large D_1 values, comparable to J, were obtained from the magnetic data fitting. The sign of zfs appears to be well determined, as in the case for **1**. Large D_1 magnitudes are expected in nickel(II) complexes of low symmetry (idealized C_{2v} here), yet the D_1 value of 36 cm^{-1} in **3** is surprisingly high; however, in the absence of EPR data, it has to be accepted. The absence of the HF EPR actually indicates a very large zfs. In addition to the parameters in Table 3, the magnetic fit yielded a TIP value of 150 × 10^{-6} emu and a mononuclear fraction f = 0.11%. DFT and UHF calculations of D in the nickel(II) complex were unsuccessful. The UHF calculation ended in error, and DFT produced a senseless, very small value. The cobalt(II) complex **3** was the most problematic in this series. In the magnetic fitting, a large TIP value of 1360 × 10^{-6} emu had to be allowed, and the fraction on mononuclear impurities (1.0%) was the highest. The self-consistent field (SCF) procedure did not converge, therefore

dx.doi.org/10.1021/ic301757g | Inorg. Chem. 2012, 51, 11820−11836

not even a rough estimate of J or D is available. DFT calculations of the exchange integrals are described separately below. Cobalt(II) might be in an orbitally degenerate state, or there might be low-lying excited states, and the entire spin Hamiltonian concept might be inapplicable, as in octahedral high-spin cobalt(II) compounds.

Magnetic Properties and EPR Spectra of $[Cu_2(\mu\text{-}F)(\mu\text{-}L_m^*)_2](BF_4)_3$ (4) and $[Cu_2(\mu\text{-}F)(\mu\text{-}L_m)_2](BF_4)_3$. Fitting of the magnetic susceptibility data (Figure 11) with eqs 8 and 10

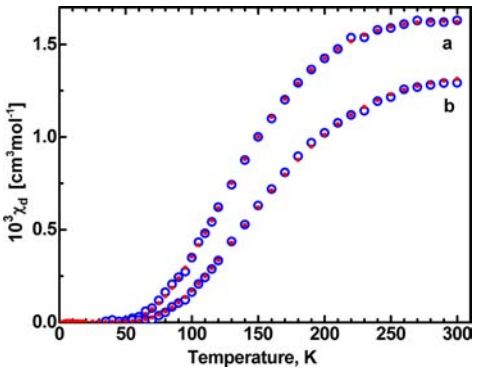

Figure 11. Magnetic susceptibility of (a) $[Cu_2(\mu\text{-}F)(\mu\text{-}L_m^*)_2](BF_4)_3$ and (b) $[Cu_2(\mu\text{-}F)(\mu\text{-}L_m)_2](BF_4)_3$ (b). Open circles, experimental data; solid dots, values calculated with (a) $g_{avg} = 2.22$, $-J = 322$ cm^{-1} and (b) $g_{avg} = 2.16$, $-J = 370$ cm^{-1}. Contributions due to mononuclear impurities were removed from experimental data according to $\chi_d = [\chi_{exp} - 2f(Ng^2\mu_B{}^2/3kT) \times 0.75]/(1 - f)$ (see eq 8). The f values used were (a) 0.015 and (b) 0.005. The original measured data are shown in the Supporting Information, Figure S10.

resulted in $J = -322$ cm^{-1} for $[Cu_2(\mu\text{-}F)(\mu\text{-}L_m^*)_2](BF_4)_3$ (**4**), $J = -340$ cm^{-1} for its perchlorate analogue,[9] and $J = -370$ cm^{-1} for $[Cu_2(\mu\text{-}F)(\mu\text{-}L_m)_2](BF_4)_3{\cdot}1.5CH_3CN$.[6] Although we have previously reported the magnetic properties of the latter, its EPR spectrum was not recorded at that time and is included here for completeness. Note that eq 10 and the spin Hamiltonian in eq 3 with $S = 1$ were used to interpret the magnetic susceptibility and EPR spectra, respectively, of the copper(II) complexes, unlike for the Mn(II), Fe(II), Co(II), and Ni(II) systems described above, which required more advanced treatment by using eqs 7−9 and the spin Hamiltonian in eq 6.

The powder samples of $[Cu_2(\mu\text{-}F)(\mu\text{-}L_m)_2](BF_4)_3{\cdot}1.5CH_3CN$ exhibited very weak and noisy EPR spectra in which the presence of two $S = 1$ species could be recognized (Figure 12), in agreement with the X-ray structure in which two independent species were detected differing in symmetry.[6b] Minuscule differences in the g parameters of the two species can only be seen thanks to the very high microwave frequency. Signals of these two species would collapse into one in standard EPR spectra.

The spectra of **4** were of yet lower quality, possibly due to the presence of several disordered molecules. Powder spectra of **4** proved to be noninterpretable, but fortunately, spectra of its frozen solution in CH_3CN at 150 K (Figure 13) allowed the extraction of the parameters $g_x = 2.15$, $g_y = 2.33$, $g_z = 2.01$, $D = 0.173$ cm^{-1}, and $E = 0.084$ cm^{-1}, similar to the values for other copper(II) complexes in this family, including that with L_m.

One of the g components in these copper(II) complexes, g_z, is very close to 2, indicating that the ground state of Cu(II) is d_{z^2}. This rarely encountered electronic configuration of

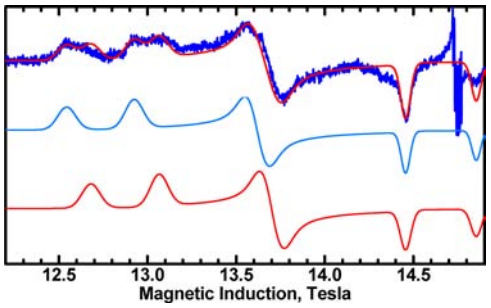

Figure 12. Top blue trace: EPR spectrum of $[Cu_2(\mu\text{-}F)(\mu\text{-}L_m)_2](BF_4)_3{\cdot}1.5CH_3CN$ recorded at 150 K with $\nu = 412.8$ GHz. The spectrum consists of two components with the following parameters of the spin Hamiltonian (eq 3) with $S = 1$: for species 1, $g_x = 2.159$, $g_y = 2.316$, $g_z = 2.013$, $D = 0.187$ cm^{-1}, and $E = 0.075$ cm^{-1}; for species 2, $g_x = 2.152$, $g_y = 2.291$, $g_z = 2.013$, $D = 0.187$ cm^{-1}, and $E = 0.075$ cm^{-1}. Spectra simulated for species 1 and 2 are plotted as blue and red traces, respectively, at the bottom. The top red trace is their sum. The spectrum of Mn(II) centered at 14.77 T ($g = 2$) is due to the gelatin cap used as a sample container. Spectra recorded with $\nu = 216.0$ GHz are shown in Figure S11 (Supporting Information).

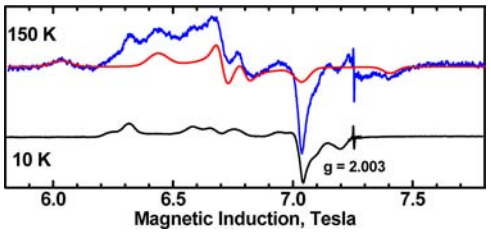

Figure 13. EPR spectra of a frozen solution of **4** in CH_3CN. Blue: experimental spectrum at 150 K and 203.2 GHz. Red: spectrum simulated with $g_x = 2.150$, $g_y = 2.329$, $g_z = 2.010$, $D = 0.173$ cm^{-1}, and $E = 0.089$ cm^{-1}. Signals due to paramagnetic impurities are seen and remain in the low-temperature spectrum (10 K, black trace), whereas signals of the dinuclear species disappear. A sharp line due to traces of a free radical is seen at $g = 2.003$.

copper(II) was also confirmed by DFT calculations. Very different magnitudes of the g_x and g_y components indicate large energy difference between the excited d_{xz} and d_{yz} orbitals of copper(II), according to the approximate formulas

$$g_x = 2.0023 - \frac{6\xi}{E(d_{z^2}) - E(d_{yz})}$$

$$g_y = 2.0023 - \frac{6\xi}{E(d_{z^2}) - E(d_{xz})}$$

$$g_z = 2.0023$$

In these formulas, ξ is the spin−orbit coupling constant, which might be reduced from its free-ion value of -828 cm^{-1} for copper(II) by the covalence effects. The zero-field splitting in a dinuclear copper(II) complex originates from the magnetic dipole−dipole interactions and from the anisotropic exchange interactions. In present case, with a Cu···Cu distance of ca. 4 Å, the dipole−dipole contribution to D cannot be more negative than -0.045 cm^{-1} (this value is appropriate for the spin Hamiltonian in eq 3 and was calculated from the point-dipole model[23,30a]), and the zero-field splitting must originate from the anisotropic exchange as in other dinuclear copper(II) systems.[21−23,30] The zero-field splitting parameters, with relatively large E compared to D in the copper(II) complexes

dx.doi.org/10.1021/ic301757g | Inorg. Chem. 2012, 51, 11820−11836

reported here as well as in ref 9, are unusual compared to other dinuclear copper(II) systems. For example, in the well-known dinuclear copper(II) carboxylates, the E parameter ranges from 0 to $\sim D/20$. It is now well understood that the exchange-related contribution to zfs in dinuclear complexes is related to the exchange coupling in the single-excited states of a dinuclear molecule, in which one of the copper(II) ions is in its ground state and the other is in one of the excited states. Only those excited states need be considered that have nonzero matrix elements of the angular momentum operator **L** with the ground state. Maurice et al. performed a sophisticated DFT analysis of such interactions in copper acetate and derived the following equations for the exchange-related D and E values[30a]

$$D = 2\frac{\xi^2 J_{x^2-y^2,xy}}{\Delta E^2_{x^2-y^2,xy}} - \frac{1}{4}\frac{\xi^2 J_{x^2-y^2,xz}}{\Delta E^2_{x^2-y^2,xz}} - \frac{1}{4}\frac{\xi^2 J_{x^2-y^2,yz}}{\Delta E^2_{x^2-y^2,yz}}$$

$$E = \frac{1}{4}\frac{\xi^2 J_{x^2-y^2,xz}}{\Delta E^2_{x^2-y^2,xz}} - \frac{1}{4}\frac{\xi^2 J_{x^2-y^2,yz}}{\Delta E^2_{x^2-y^2,yz}}$$

Symbols such as $J_{x^2-y^2,xz}$ are the exchange integrals between the $d_{x^2-y^2}$ ground orbital of one copper(II) ion and the d_{xz} orbital of another copper(II). (Note that, in the above equations, positive J is considered antiferromagnetic.[30]) In the copper acetate case, axis z joins the two copper(II) ions, and the d_{xz} and d_{yz} orbitals of one copper(II) are oriented similarly compared to the $d_{x^2-y^2}$ orbital of another copper(II) atom. Accordingly, the terms in the equations above involving $J_{x^2-y^2,xz}$ and $J_{x^2-y^2,yz}$ must be of similar magnitude,[30a] resulting in a small or approximately zero E parameter. Also, the g_x and g_y components are close to each other because of the similarity in the d_{xz} and d_{yz} arrangements.

In our case, with d_{z^2} being the ground state, only the d_{xz} and d_{yz} orbitals can play a role (as they have nonzero matrix elements of **L** with d_{z^2}). The z axis is along the vertical bipyramid axis, whereas x joins the copper(II) ions. The d_{xz} orbital of one copper extends two of its lobes toward the bridge and forms a π bond to F^-, but the d_{yz} orbital (perpendicular to the Cu−F direction) cannot form bonds with F^-. It thus seems logical to assume that the d_{xz}−d_{z^2} interaction affects the zfs in our copper complex more than the d_{yz}−d_{z^2} interaction. These two interactions contribute to the D_{yy} and the D_{xx} components of the interaction tensor, respectively (because $|\langle d_{z^2}|\mathbf{L}_y|d_{xz}\rangle|^2 = |\langle d_{z^2}|\mathbf{L}_x|d_{yz}\rangle|^2 = 3$). To extract the exchange-related part of the zfs parameters, one subtracts the calculated dipole−dipole contribution from the experimental EPR parameters. This requires knowledge of the sign of the experimental D parameter,[23] which could not be determined here. Also, the point-dipole model gives very inaccurate results.[30a] Nevertheless, assuming negative D, it is possible to estimate the exchange-related components of the zfs tensor $D_{xx}(\text{ex}) = 0.13$ cm^{-1}, $D_{yy}(\text{ex}) = 0.26$ cm^{-1}, and $D_{zz}(\text{ex}) = 0$ (see the Supporting Information), which result in the scalar values $D_{\text{ex}} = -0.195$ cm^{-1} and $E_{\text{ex}} = -0.065$ cm^{-1} (pertinent to the spin Hamiltonian in eq 3).

DFT Calculation of the Exchange Integrals. We have attempted to estimate the exchange integrals by "broken-symmetry" density functional theory (DFT) calculations.[31] The molecules were simplified by removing the methyl groups on pyrazole fragments as well as the benzene rings and placing hydrogen atoms at appropriate locations. All remaining atoms were retained at the crystallographic positions. The system of coordinates was chosen so that the x axis was along the metal−F vector and the z axis was perpendicular to the plane of the fluoride and two equatorial nitrogen atoms. The broken-symmetry procedure applied to a system of two metal ions, A and B, each containing N unpaired spins, first performs a self-consistent field (SCF) calculation for a high-spin (HS) molecule with spin equal to N. In the next stage, another SCF calculation is performed taking all spins on atom A to be up and all spins on atom B to be down, which is referred to as the broken-symmetry (BS) solution. Finally, the magnitude of J (for the Hamiltonian in eq 1) is evaluated as $J = 2(E_{\text{HS}} - E_{\text{BS}})/(\langle S^2\rangle_{\text{HS}} - \langle S^2\rangle_{\text{BS}})$, where E are the energies and $\langle S\rangle^2$ are the expectation values of the spin-squared operator in the HS and BS states.

The Ahlrichs-type basis set TZVPP[32a] for the metals and all coordinated atoms, and the SVP basis set[33] for other atoms were used, combined with the B3LYP[33] functional. Ahlrichs polarization functions from basis H−Kr R and auxiliary bases from the TurboMole library were also used.[32b] The SCF calculations did not converge in the case of the cobalt(II) complex. The results obtained in the other cases appear to be reasonable. The correct sign of J was found, but the magnitude was overestimated except for the copper(II) complex (Table 3). The interactions that contribute to the antiferromagnetism of dinuclear complexes involve pairs of overlapping "magnetic orbitals" localized on both metal ions. Representative orbitals are plotted in Figure 15 and Figures S12 and S13 (Supporting Information). Various metal orbitals have very different abilities, dictated by symmetry, to interact with the bridging atom, and as a result, their relative importance in transmitting the exchange interactions, measured by the overlap integral[34] of the magnetic orbitals, is also very unequal.

The d^9 copper(II) complex **4** is best to describe first. As was done previously by Hay et al.[8b] for a different bridging system, in this trigonal bipyramidal geometry with the coordinates chosen as above, the magnetic orbital has mainly d_{z^2} character. The calculations show that the key orbitals influencing the magnetic properties are the symmetric antibonding combination formed by the magnetic orbitals of the metal (mainly consisting of the metal d orbitals, but delocalized onto the ligands) with the s orbitals and the antisymmetric antibonding combination with the p_x orbital of the bridging group (Figure 14). The p_x orbital interacts more strongly, so the antisymmetric orbital is relatively high in energy, stabilizing the singlet state and producing the large $-J$ values. The calculated energy difference between the antisymmetric and symmetric orbitals containing the d_{z^2} orbitals of two copper(II) ions is 0.532 eV (4290 cm^{-1}, average for the spin-up and spin-down energies).

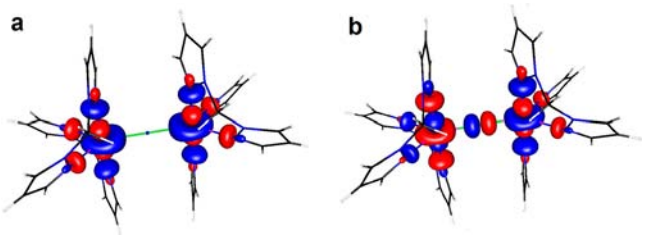

Figure 14. (a) Symmetric and (b) antisymmetric antibonding combinations of the copper(II) d_{z^2} orbitals with the bridging F^- orbitals of appropriate symmetry (s and p, respectively) in the model compound $[Cu_2(\mu\text{-F})(\text{bis(1-pyrazolyl)methane})_4]^{3+}$.

dx.doi.org/10.1021/ic301757g | Inorg. Chem. 2012, 51, 11820−11836

In the multielectron ions Mn(II), Fe(II), Co(II), and Ni(II) studied here, there are more contributions to the exchange interactions, which are associated with the symmetric and antisymmetric combinations involving other d orbitals of the two metal ions; the four combinations for nickel(II) are shown in Figure S14 (Supporting Information). Analysis of the broken-symmetry results indicates that the energy of the symmetric (s) and antisymmetric (a) orbitals increase in the sequence $yz(s) < yz(a) < x^2 - y^2(s) < xz(s) < x^2 - y^2(a) < xz(a) < xy(s) < xy(a) < z^2(s) < z^2(a)$ for the manganese(II) complex and in the sequence $yz(s) < yz(a) < x^2 - y^2(s) < xz(s) < xz(a) < x^2 - y^2(a) < xy(s) < xy(a) < z^2(s) < z^2(a)$ for the iron(II) complex. Only the last of the orbitals listed here contain an unpaired electron in the case of copper(II), whereas xy and z^2 are the SOMOs (singly occupied molecular orbitals) for nickel(II), all except yz are SOMOs for iron(II), and finally each of the five d orbitals contains one unpaired electron in manganese(II). The cobalt(II) complex will not be discussed here because the DFT calculations failed in this case. The d_{yz} metal orbitals cannot interact with the bridging atom, and thus, the energies of the symmetric and antisymmetric combinations will be almost the same, resulting in no contribution to the antiferromagnetic exchange in the only case where yz has to be considered, that is, in the manganese(II) complex.

The situation is relatively simple in the nickel(II) complex, because the d_{z^2} and d_{xy} SOMOs do not interfere with each other: the former engages only in the σ bonds, and the latter engages only in π bonds to the bridging ligand. The two magnetic orbitals are pure, and their respective d_{z^2} and d_{xy} characters are easily recognizable (Figure 15).

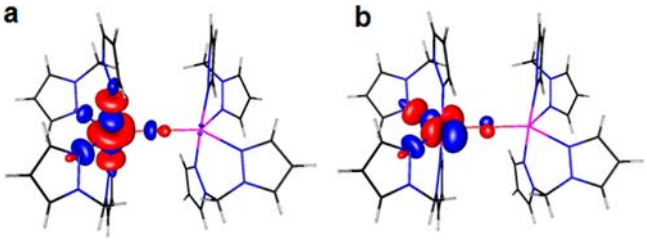

Figure 15. (a) d_{z^2} and (b) d_{xy} characters of the magnetic orbitals for the model compound $[Ni_2(\mu\text{-F})(\text{bis(1-pyrazolyl)methane})_4]^{3+}$.

In the iron(II) and manganese(II) complexes, a $d_{x^2-y^2}$ SOMO is also present. It engages in σ bonds with the bridging fluoride, and the resulting magnetic orbital, being a mixture of d_{z^2} and $d_{x^2-y^2}$, does not exhibit a readily recognizable shape. Note that the magnetic orbitals in parts a and d in Figure S12 (Supporting Information) for iron(II) and Figure S13 (Supporting Information) for manganese(II) are these mixed ones. In the antisymmetric or symmetric combinations, the d_{z^2} and $d_{x^2-y^2}$ shapes are seen, but in the magnetic orbitals, they are combined. An important quantity allowing the contribution of an exchange pathway to the overall antiferromagnetic interaction to be assessed is the overlap integral between the magnetic orbitals of two interacting metal ions. Table 4 shows that the magnetic orbitals engaged in σ bonds to the bridging ligand contribute the most to the exchange interactions. The calculated exchange integrals were in half-quantitative agreement with the experiment, being significantly too large (except for the copper(II) case). Often, an empirical factor of 0.5 is applied to the exchange integral values calculated by DFT,[35] and indeed, this would result in a better agreement between our calculated and experimental J values (except for the Cu(II) complex **4**). We do not introduce such a factor here, however.

Table 4. Spin Densities and Orbital Interactions As Calculated by the Broken-Symmetry DFT Method

	metal in the complex			
	Mn(II)	Fe(II)	Ni(II)	Cu(II)
	Spin Density			
metal d_{yz}	0.979	0.080	0.008	0.008
metal d_{xz}	0.967	0.960	0.005	0.001
metal $d_{x^2-y^2}$	0.951	0.910	0.019	0.025
metal d_{xy}	0.927	0.908	0.867	0.009
metal d_{z^2}	0.904	0.851	0.791	0.663
F p_x	0.013	0.027	0.030	0.035
F p_y	0.021	0.024	0.030	0.000
F p_z	0.018	0.020	0.000	0.000
	$E_{anti} - E_{sym}$[a] (eV)			
yz	0.014	–	–	–
xz	0.267	0.299	–	–
$x^2 - y^2$	0.176	0.336	–	–
xy	0.339	0.303	0.265	–
z^2	0.417	0.276	0.421	0.532
	Overlap Integral between the Magnetic Orbitals (S)			
yz	0	–	–	–
xz	0.037	–	–	–
$x^2 - y^2$	b	b	–	–
xy	0.049	0.046	0.042	–
z^2	0.084[b]	0.100[b]	0.075	0.125
	Exchange Integral (J)			
calculated, DFT	−14	−28	−55	−380
experimental	−6.7	−16.3	−39	−322

[a]Calculated from the averages of the spin-up and spin-down energies of the respective antisymmetric and symmetric orbitals. [b]$x^2 - y^2$ and z^2 magnetic orbitals are combined.

The differences between the antisymmetric and symmetric combinations in Table 4 are similar for all metals (for the orbitals of the same type), and the overlap integrals are similar, yet the exchange integrals are very different. The relations between the exchange integrals and the orbital energies involve the square of the number of unpaired electrons, n^2.[8b] When the J values in Table 4 are multiplied by n^2, the resulting numbers are of the same order of magnitude.

DISCUSSION

The preparation of the new third-generation ligand $\mathbf{L_m}$*, containing 3,5-dimethyl group substitution on the pyrazolyl rings, has allowed the syntheses of seven dinuclear cations of the formula $[M_2(\mu\text{-F})(\mu\text{-}\mathbf{L_m}^*)_2]^{3+}$ [M = Mn(II), Fe(II), Co(II), Ni(II), Cu(II), Zn(II), and Cd(II)], all with essentially the same metallacyclic structure containing a linear M−F−M core, a virtually unknown arrangement in dinuclear complexes prior to this work. Although we previously prepared analogous complexes with the unsubstituted ligand $\mathbf{L_m}$, only the M = Fe(II), Co(II), Cu(II), and Zn(II) complexes could be prepared; dibridged $[M_2(\mu\text{-F})_2(\mu\text{-}\mathbf{L_m}^*)_2]^{2+}$ formed with the metals Ni(II) and Cd(II). Clearly, the difference in the two systems relates to the steric influence of the 3,5-dimethyl groups, where space-filling models (Figure S15, Supporting Information) show the methyl groups in the metallacycles are close to each other and the linking arene groups. This conclusion is supported by the unusual chemical shifts reported for one set of methyl resonances in both the ^{1}H and ^{13}C NMR

dx.doi.org/10.1021/ic301757g | Inorg. Chem. 2012, 51, 11820−11836

spectra. In this substituted system, dibridging fluoride is sterically blocked. Steric effects also support the axially compressed trigonal bipyramidal geometry around the metal centers over the more favored apically elongated square pyramidal,[36,37] where the severe compression of the axial bond lengths in $[Cu_2(\mu\text{-}F)(\mu\text{-}\mathbf{L}_m\text{*})_2]^{3+}$ is explained, in addition, by the pseudo-Jahn–Teller (PJT) effect.[38]

The most obvious trend in comparing the $[M_2(\mu\text{-}F)(\mu\text{-}\mathbf{L}_m\text{*})_2]^{3+}$ structures of the six first-row metals is the lack of trends in the overall geometry of the metals and the M–F bond lengths. Scheme 3 shows a plot of the predicted[17] and actual

Scheme 3. Plot of the Metal(II) Cations (Listed in Order of Increasing *Z*) versus Predicted M–F and M–N Bond Distances (Based on Ionic Radii) and Observed M–F [Average for Mn(II)] and Average M–N Bond Distances in Compounds 1–5 and 7

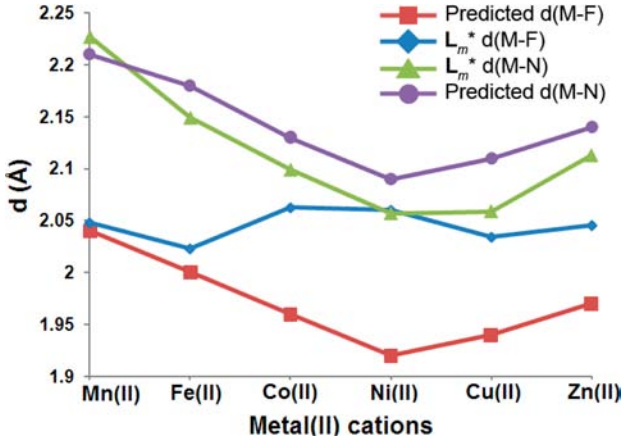

M–F and average M–N bond lengths. The changes in the M–N bond lengths track those predicted from the change in ionic radii of the metal(II) cation, although with the exception of manganese(II), all are somewhat shorter. In contrast, the actual M–F bond lengths are nearly constant, within 0.04 Å, with the longest recorded for nickel(II), even though it is the smallest cation.[17] Clearly, the M–F or more exactly M–F–M lengths are being slightly elongated, with the exception of the largest metal manganese(II), and held constant by the bridging $\mathbf{L}_m$* ligands. The same trends were observed previously in the $\mathbf{L}_m$ system, where the M–F bond lengths also vary by only 0.04 Å and do not track the metal ionic radii. Importantly, the overall M–F average in the $\mathbf{L}_m$ system is 1.96 Å, 0.09 Å shorter than the 2.05-Å average for the $\mathbf{L}_m$* system. This difference is again explained by the increased steric crowding in the $\mathbf{L}_m$* system. As with manganese(II), the Cd–F bond length in $[Cd_2(\mu\text{-}F)(\mu\text{-}\mathbf{L}_m\text{*})_2]^{3+}$ matches that predicted for the larger cadmium(II) ion. The larger size of these two metals "fits" the favored M–F–M distance of the $\mathbf{L}_m$* ligands. It is the elongated M–F distances for the other metals, forced by the $\mathbf{L}_m$* ligands, that explains the observed contracted M–N distances shown in Scheme 3.

There are very few previous examples of dinuclear complexes with linear or nearly linear single-fluoride bridges for comparison. A zinc(II) bimetallic complex bonded to a ligand containing a 1,3-substituted pyridine with bis(imidazolyl)-methylene donor groups contains a linear M–F–M arrangement in a discrete dinuclear complexes where the Zn–F distance is 1.99 Å, close to the predicted value.[39] Three other octahedral complexes, one of copper(II)[40] and two of nickel(II),[41,42] with M–F–M angles ranging from 161° to 177° have been reported. Our ability to prepare this extensive series of complexes with this unique linear M–F–M arrangement is forced/supported by the third-generation bis-(pyrazolyl)methane ligand reported in this work, the bulky $\mathbf{L}_m$*.

It is interesting to compare the structural behavior of the copper(II) $\mathbf{L}_m$ and $\mathbf{L}_m$* compounds with those of other Cu(II)[bis(pyrazolyl)methane]$_2$ compounds, the metal that has the largest number of known complexes of this type. The parent $H_2C(pz)_2$ ligand forms six-coordinate $[Cu[H_2C(pz)_2]_2Cl(H_2O)]^+$ with all four pyrazolyl rings in the equatorial positions of an octahedron.[43] Copper(II) compounds with bulkier bis(pyrazolyl)methane ligands, such as $[Cu[H_2C(3,5\text{-}Me_2pz)_2]_2Cl]_2(CuCl_4)$,[44] $[Cu[H_2C(3,5\text{-}Me_2pz)_2]_2(CH_3OH)](ClO_4)_2$,[44] and $[Cu_2[H_2C(3,5\text{-}Me_2pz)_2]_4(ta)](ClO_4)_2$[45] ($H_2ta$ = terephthalic acid), form axially elongated square pyramidal geometries around the copper(II) center, with three pyrazolyl rings in the equatorial plane and one in the axial position (with τ_5 values of 0.04–0.47). As the steric crowding of the complex is increased, upon using isopropyl-substituted pyrazolyl groups, as in $[Cu([H_2C(3\text{-}i\text{-}Pr\text{-}pz)_2])_2(H_2O)]_2(ClO_4)_2$,[44] the geometry around the copper(II) changes from axially elongated square pyramidal to axially compressed trigonal bipyramidal geometry (τ_5 = 0.64, Cu–N_{ax} = 1.940 Å, Cu–N_{eq} = 2.174 Å). Thus, as the steric interactions built into the ligands increase, the copper(II) coordination changes from octahedral to square pyramidal to trigonal bipyramidal geometry. The bulky third-generation bis(pyrazolyl)methane ligands $\mathbf{L}_m$ and especially $\mathbf{L}_m$* stabilize the metallacycle and the less stable compressed trigonal bipyramidal arrangement.

The NMR studies clearly indicate these metallacycles hold structure in solution. Most definitive on this issue are the ^{19}F and ^{113}Cd spectra of the $[Cd_2(\mu\text{-}F)(\mu\text{-}\mathbf{L}_m\text{*})_2]^{3+}$ cation that show appropriate chemical shifts[3d] and coupling expected for the Cd–F–Cd core arrangement and the two sets of ^1H and ^{13}C pyrazolyl ring resonances expected from the solid-state structures. The stability of the metallacycles is also highlighted by the positive-ion electrospray mass spectra of all seven complexes that show clusters such as $[M_2(\mathbf{L}_m\text{*})_2F(A)_2]^+$ (A = BF_4^- or ClO_4^-) and $[M_2(\mathbf{L}_m\text{*})_2F]^{3+}$.

Both copper(II) $[Cu_2(\mathbf{L})_2F]^{3+}$ metallacycles, with $\mathbf{L}$ = $\mathbf{L}_m$ and $\mathbf{L}_m$*, represent the first examples of linear single-fluoride-bridged dinuclear compounds, where copper(II) is in this unusual, axially compressed trigonal bipyramidal coordination environment. This architecture leads to substantial antiferromagnetic interactions, J = −370 and −322 cm^{-1} respectively, comparable to those measured in copper(II) acetate dimers[46] (usually J is between −300 and −350 cm^{-1}). For comparison, Noro and co-workers[40] recently reported $[Cu_2F(BF_4)_3(4\text{-}phpy)_7]$ (4-phpy = 4-phenylpyridine) where the axially elongated octahedral Cu(II) centers, linearly bridged by F^- (Cu1···Cu2 = 4.12 Å, Cu1–F–Cu2 = 177.5°), are orthogonally positioned with respect to each other (Jahn–Teller axes of Cu1 and Cu2 are not parallel), resulting in ferromagnetic interactions (J = +13.2 cm^{-1}). Another example of a bent monofluoride-bridged copper(II) compound (Cu1–F–Cu2 = 115.12°) from the Christou group,[47] $[Cu_2F(OAc)_2L]BF_4$, L = 1,2-bis(2,2′-bipyridil-6-yl)ethane, places the copper(II) centers in a square pyramidal coordination environment. Because of the counter complementarity of the bridging ligands, ferromagnetic behavior was again observed (J = +15.6 cm^{-1}).

dx.doi.org/10.1021/ic301757g | Inorg. Chem. 2012, 51, 11820–11836

Few data exist for the other metals. Antiferromagnetic superexchange interactions with a magnitude similar to that observed in $3{\cdot}2H_2O$ (J = −39.0 cm^{-1}) were reported for $[Ni_2(L)_2F](BF_4)_3$,[41] L = 2,5,8-trithia[9],(2,9)-1,10-phenanthrolinophane, one of the two[42] dinuclear compounds with almost linear fluoride bridges with other metals. The nickel(II) centers are in a distorted octahedral coordination environment (Ni···Ni′ = 3.887 Å, Ni−F−Ni′ = 161.31°), and J is −40 cm^{-1}.

The theory of the isotropic exchange interactions in dinuclear and polynuclear complexes is well understood. Antiferromagnetic interactions are transmitted through the magnetic orbitals localized on individual metal ions, provided that these magnetic orbitals overlap. Interactions between nonoverlapping orbitals lead to ferromagnetic contributions. The broken-symmetry method, developed to calculate the exchange integrals, is becoming a standard tool of coordination chemistry. DFT calculations in this work reproduced the experimental J values semiquantitatively and allowed identification of the orbital interactions that contribute to the exchange interactions. The magnetic results reported here represent the first test of the theory for a series of complexes of different metals in dinuclear complexes with linear M−F−M bridges. Both theory and experimental results show that the trend is increasing antiferromagnetic coupling interactions as one moves to the right across the periodic table from manganese(II) to copper(II), with the interaction for copper(II) being much larger.

The zero-field splitting (zfs) is a much more complicated problem. Even in mononuclear complexes of metal ions with $S > {}^1/_2$, the theoretical calculation of the zfs parameters is still a challenge. This zfs, in the form of D_1, provides the bulk of the zero-field splitting in dinuclear complexes of multielectron ions, as seen in our manganese(II) and iron(II) complexes. Because of its magnitude, it also renders such complexes unsuitable for standard X- or Q-band EPR techniques. The spectrum of our dinuclear iron(II) complex (Figure 10) appears to be the first one where the allowed transitions between states split by D are directly observed, a result of the application of very high microwave frequencies and magnetic fields in this study.

In the theoretical calculations, the interaction term D_{12} is a greater challenge yet than D_1. It contains both the magnetic dipolar interaction and the anisotropic exchange interaction, which is a contribution mediated by the spin−orbit coupling and is the most difficult to evaluate by theory. To our knowledge, only one successful calculation of D_{12} (in copper acetate) has been reported so far.[30a]

CONCLUSIONS

The new ditopic ligand *m*-bis[bis(3,5-dimethyl-1-pyrazolyl)-methyl]benzene ($\mathbf{L}_m$*) has been prepared and used to synthesis the series of metal complexes $[M_2(\mu\text{-}F)(\mu\text{-}\mathbf{L}_m^*)_2]^{3+}$ [M = Mn(II), Fe(II), Co(II), Ni(II), Cu(II), Zn(II), and Cd(II)] that have metallacyclic structures and are the first series with the linear M−F−M core. The metal ions are all in a distorted trigonal bipyramidal geometry in the solid state, an arrangement that is maintained in solution. The bridging ditopic ligands cause the M−F bond lengths to remain nearly constant despite the changes in the ionic radii of the cations along the series. The paramagnetic compounds with the metals from manganese(II) to copper(II) are antiferromagnetically coupled, with the magnitude of the coupling increasing along the series from left to right across the periodic table; the coupling is very large for copper(II), −322 cm^{-1}. The spin Hamiltonian parameters, determined from the high-frequency EPR spectra of the manganese(II) and iron(II) complexes, showed that the zero-field splitting in the dinuclear systems is mainly caused by the zfs splitting on single ions. In the copper(II) complexes, the zfs is dominated by the anisotropic exchange interactions. The lack of axial symmetry of the latter and of the EPR g factor can be understood by considering the arrangement of the copper(II) d_{xz} and d_{yz} orbitals with respect to the bridging fluoride. Both the magnetic and EPR data are supported by DFT calculations. Further work is planned on these linearly bridged binuclear complexes using the $\mathbf{L}_m$* ligand, including systems bridged by OH^- and Cl^-.

ASSOCIATED CONTENT

Supporting Information

X-ray crystallographic files in CIF format, description of the X-ray structural analysis, table of bond lengths, additional information related to the magnetic and EPR data, results of the broken-symmetry DFT calculations, space-filling models. This material is available free of charge via the Internet at http://pubs.acs.org.

AUTHOR INFORMATION

Corresponding Author

*E-mail: reger@mailbox.sc.edu (D.L.R.), ozarowsk@magnet.fsu.edu (A.O.).

Notes

The authors declare no competing financial interest.

ACKNOWLEDGMENTS

The authors acknowledge with thanks the financial support of the National Science Foundation through Grant CHE-1011736. The high-field EPR spectra were recorded at the NHMFL, which is funded by the NSF through Cooperative Agreement DMR-0654118, the State of Florida, and the U.S. Department of Energy. We are also grateful to Ministry of Science and Higher Education of the Polish Republic for financial support in the purchase of the Bruker ELEXSYS E 500 EPR spectrometer.

REFERENCES

(1) (a) Zhao, D.; Timmons, D. J.; Yuan, D.; Zhou, H.-C. *Acc. Chem. Res.* **2011**, *44*, 123. (b) Northrop, B. H.; Yang, H.-B.; Stang, P. J. *Chem. Commun.* **2008**, *45*, 5896. (c) Chen, C.-L; Zhang, J.-Y.; Su, C.-Y *Eur. J. Inorg. Chem.* **2007**, 2997. (d) Dul, M.-C.; Pardo, E.; Lescouëzec, R.; Journaux, Y.; Ferrando-Soria, J.; Ruiz-García, R.; Cano, J.; Julve, M.; Lloret, F.; Cangussu, D.; Pereira, C. L. M.; Stumpf, H. O.; Pasán, J.; Ruiz-Pérez, C. *Coord. Chem. Rev.* **2010**, *254*, 2281. (e) Pariya, C.; Fronczek, F. R.; Maverick, A. W. *Inorg. Chem.* **2011**, *50*, 2748. (f) Clegg, J. K.; Bray, D. J.; Gloe, K.; Hayter, M. J.; Jolliffe, K.; Lawrance, G. A.; Meehan, G. V.; McMurtrie, J. C.; Lindoy, L. F.; Wenzel, M. *Dalton Trans.* **2007**, 1719. (g) Su, C.-Y.; Cai, Y.-P.; Chen, C.-L.; Smith, M. D.; Kaim, W.; zur Loye, H.-C. *J. Am. Chem. Soc.* **2003**, *125*, 8595.

(2) (a) Reger, D. L.; Foley, E. A.; Smith, M. D. *Inorg. Chem. Commun.* **2010**, *13*, 568. (b) Reger, D. L.; Foley, E. A.; Semeniuc, R. F.; Smith, M. D. *Inorg. Chem.* **2007**, *46*, 11345. (c) Reger, D. L.; Gardinier, J. R.; Bakbak, S.; Semeniuc, R. F.; Bunz, U. H.; Smith, M. D. *New J. Chem.* **2005**, *29*, 1035.

(3) (a) Titze, C.; Hermann, J.; Vahrenkamp, H. *Chem. Ber.* **1995**, *128*, 1095. (b) Reger, D. L.; Elgin, J. D.; Foley, E. A.; Smith, M. D.; Grandjean, F.; Long, G. J. *Inorg. Chem.* **2009**, *48*, 9393. (c) Reger, D. L.; Grattan, T. C.; Brown, K. J.; Little, C. A.; Lamba, J. J. S.; Rheingold,

A. L.; Sommer, R. D. J. *Organomet. Chem.* **2000**, *607*, 120. (d) Weis, K.; Vahrenkamop, H. *Inorg. Chem.* **1997**, *36*, 5592.
(4) (a) Reger, D. L.; Watson, R. P.; Smith, M. D.; Pellechia, P. J. *Cryst. Growth Des.* **2007**, *7*, 1163. (b) Reger, D. L.; Watson, R. P.; Gardinier, J. R.; Smith, M. D. *Inorg. Chem.* **2004**, *43*, 6609. (c) Reger, D. L.; Watson, R. P.; Smith, M. D. *J. Chem. Crystallogr.* **2008**, *38*, 17. (d) Reger, D. L.; Semeniuc, R. F.; Smith, M. D. *Dalton Trans.* **2008**, 2253.
(5) (a) Reger, D. L.; Watson, R. P.; Smith, M. D. *J. Organomet. Chem.* **2007**, *692*, 5414. (b) Reger, D. L.; Watson, R. P.; Smith, M. D. *J. Organomet. Chem.* **2007**, *692*, 3094. (c) Reger, D. L.; Watson, R. P.; Smith, M. D.; Pellechia, P. J. *Organometallics* **2005**, *24*, 1544.
(6) (a) Reger, D. L.; Watson, R. P.; Smith, P. J. *Inorg. Chem.* **2006**, *45*, 10077. (b) Reger, D. L.; Foley, E. A.; Watson, R. P.; Pellechia, P. J.; Smith, M. D. *Inorg. Chem.* **2009**, *48*, 10658. (c) Reger, D. L.; Foley, E. A.; Watson, R. P.; Pellechia, P. J.; Smith, M. D. *Inorg. Chem.* **2011**, *50*, 2704. (d) Reger, D. L.; Watson, R. P.; Gardinier, J. R.; Smith, M. D.; Pellechia, P. J. *Inorg. Chem.* **2006**, *45*, 10088. (e) Reger, D. L.; Foley, E. A.; Smith, M. D. *Inorg. Chem.* **2009**, *48*, 936.
(7) Selected examples: (a) Nadeem, M. A.; Bhadbhade, M; Stride, J. A. *Dalton Trans.* **2010**, *39*, 9860. (b) Ding, K.; Dugan, T. R.; Brennessel, E. B.; Holland, P. L. *Organometallics* **2009**, *28*, 6650. (c) Vela, J.; Smith, J. M.; Yu, Y.; Ketterer, N. A.; Flaschenriem, C. J.; Lachicotte, R. J.; Holland, P. L. *J. Am. Chem. Soc.* **2005**, *127*, 7857. (d) Zhu, Q.; Nelson, K. J.; Shum, W. W.; DiPasquale, A.; Rheingold, A. L.; Miller, J. S. *Inorg. Chim. Acta* **2009**, *362*, 595. (e) Birk, T.; Magnussen, M. J.; Piligkos, S.; Weihe, H.; Holten, A.; Benidx, J. *J. Fluorine Chem.* **2010**, *131*, 898. (f) Tomat, E.; Cuesta, L.; Lynch, V. M.; Sessler, J. L. *Inorg. Chem.* **2007**, *46*, 6224. (g) Casellas, H.; Pevec, A.; Kozlevčar; Gamez, P.; Reedijk, J. *Polyhedron* **2005**, *24*, 1549. (h) Wang, C.-M.; Liao, C.-H.; Kao, H.-M.; Lii, K.-H. *Inorg. Chem.* **2005**, *44*, 6294. (i) Leo, R.; Massa, W.; Pebler, J. *J. Fluorine Chem.* **2004**, *125*, 923. (j) Choudhury, A.; Rao, C. N. R. *J. Struct. Chem.* **2002**, *43*, 632. (k) Worm, K.; Chu, F.; Matsumoto, K; Best, M. D.; Lynch, V.; Anslyn, E. V. *Chem.—Eur. J.* **2003**, *9*, 741. (l) Blake, A. J.; Devillanova, F. A.; Garau, A.; Harrison, A.; Isaia, F.; Lippolis, V.; Tiwary, S. K.; Schröder, M.; Verani, G.; Whittaker, G. *J. Chem. Soc., Dalton Trans.* **2002**, 4389.
(8) (a) Kahn, O. *Molecular Magnetism*; VCH Publishers, Inc.: New York, 1993. (b) Hay, P. J.; Thibeault, J. C.; Hoffmann, R. *J. Am. Chem. Soc.* **1975**, *97*, 4884.
(9) Reger, D. L.; Pascui, A. E.; Smith, M. D.; Jezierska, J.; Ozarowski, A. *Inorg. Chem.* **2012**, *51* (15), 7966.
(10) Hassan, A. K.; Pardi, L. A.; Krzystek, J.; Sienkiewicz, A.; Goy, P.; Rohrer, M.; Brunel, L.-C. *J. Magn. Reson.* **2000**, *142*, 300.
(11) (a) O'Connor, C. J. *Prog. Inorg. Chem.* **1982**, *29*, 203. (b) Bain, G. A.; Berry, J. F. *J. Chem. Educ.* **2008**, *85*, 532.
(12) (a) Barbour, L. J *J. Supramol. Chem.* **2003**, *1*, 189. (b) *POV-RAY 3.6*; Persistence of Vision Raytracer Pty Ltd.: Williamstown, Victoria, Australia, 2006. (c) *MestReNOVA v.5.2.5*; Mestrelab Research S.L.: Santiago de Compostela, Spain, 2008. (d) Laaksonen, L. *gOpenMol version 3.00*; CSC - IT Center for Science Ltd.: Espoo, Finland, 2005; available at www.csc.fi/english/pages/g0penMol.
(13) (a) *SMART Version 5.630*; Bruker Analytical X-ray Systems, Inc.: Madison, WI, 2003. (b) *SAINT+ Version 6.45*; Bruker Analytical X-ray Systems, Inc.: Madison, WI, 2003. (c) *SADABS Version 2.10*; Bruker Analytical X-ray Systems, Inc.: Madison, WI, 2003.
(14) Sheldrick, G. M. *Acta Crystallogr. A* **2008**, *64*, 112.
(15) Peterson, L. K.; Kiehlmann, E.; Sanger, A. R.; Thé, K. I. *Can. J. Chem.* **1974**, *52*, 2367.
(16) Addison, A. W.; Rao, T. N.; Reedijk, J.; Van Rijn, J.; Verschoor, G. C. *J. Chem. Soc., Dalton Trans.* **1984**, 1349.
(17) Shannon, R. D *Acta Crystallogr. A* **1976**, *32*, 751.
(18) (a) Kepert, D. L. In *Inorganic Chemistry Concepts*; Springer-Verlag: New York, 1982; Vol. *6*, p 36. (b) Pearson, R. G. *J. Am. Chem. Soc.* **1969**, *91* (18), 4947. (c) Pearson, R. G. *Proc. Natl. Acad. Sci. U.S.A.* **1975**, *72* (6), 2104. (d) Bartell, L. S. *J. Chem. Educ.* **1963**, *45*, 754.
(19) Zabrodsky, H.; Peleg, S.; Avnir, D. *J. Am. Chem. Soc.* **1993**, *115*, 8278.
(20) (a) Spek, A. L. *Acta Crystallogr. A* **1990**, *46*, C34. (b) Spek, A. L. *PLATON, A Multipurpose Crystallographic Tool*; Utrecht University: Utrecht, The Netherlands, 1998.
(21) Bencini, A.; Gatteschi, D. *EPR of Exchange Coupled Systems*; Springer Verlag: Berlin, 1990.
(22) Abragam, A.; Bleaney, B. *Electron Paramagnetic Resonance of Transition Ions*; Clarendon Press: London, 1970.
(23) Ozarowski, A. *Inorg. Chem.* **2008**, *47*, 9760.
(24) Neese, F. *ORCA: An Ab Initio Density Functional and Semiempirical Program Package*, version 2.8; Universität Bonn: Bonn, Germany, 2008; free download available from http://www.thch.uni-bonn.de/tc/orca/, registration required.
(25) (a) Krzystek, J.; Ozarowski, A.; Zvyagin, S. A.; Telser, J. *Inorg. Chem.* **2012**, *51*, 4954. (b) Wojciechowska, A.; Daszkiewicz, M.; Staszak, Z.; Trusz-Zdybek, A.; Bienko, A.; Ozarowski, A. *Inorg. Chem.* **2011**, *50*, 11532. (c) Garribba, E.; Micera, G. *J. Chem. Educ.* **2006**, *83*, 1229.
(26) Mantel, C.; Baffert, C.; Romero, I.; Deronzier, A.; Pecaut, J.; Collomb, M.-N.; Duboc, C. *Inorg. Chem.* **2004**, *43*, 6455.
(27) Hendrich, M. P.; Day, E. P.; Wang, C.-P.; Synder, B. S.; Holm, R. H.; Münck, E. *Inorg. Chem.* **1994**, *33*, 2848.
(28) Harman, W. H.; Harris, T. D.; Freedman, D. E.; Fong, H.; Chang, A.; Rinehart, J. D.; Ozarowski, A.; Sougrati, M. T.; Grandjean, F.; Long, G. J.; Chang, C. J. *J. Am. Chem. Soc.* **2010**, *132*, 18115.
(29) (a) Solomon, E. I.; Brunold, T. C.; Davis, M. I.; Kemsley, J. N.; Lee, S. K.; Lehnert, N.; Neese, F.; Skulan, A. J.; Yang, Y. S.; Zhou, J. *Chem. Rev.* **2000**, *100*, 235. (b) Yang, Yi-S.; Broadwater, J. A.; Coates Pulver, S.; Fox, B. G.; Solomon, E. I. *J. Am. Chem. Soc.* **1999**, *121*, 2770. (c) Solomon, E. I.; Pavel, E. G.; Loeb, K. E.; Campochiaro, C. *Coord. Chem. Rev.* **1995**, *144*, 369.
(30) (a) Maurice, R.; Sivalingam, K.; Ganyushin, D.; Guihery, N.; de Graaf, C.; Neese, F. *Inorg. Chem.* **2011**, *50*, 6229. (b) Ozarowski, A.; Szymanska, I. B.; Muziol, T.; Jezierska, J. *J. Am. Chem. Soc.* **2009**, *131*, 10279. (c) Gribnau, M. C. M.; Keijzers, C. P. *Inorg. Chem.* **1987**, *26*, 3413. (d) Ross, P. K.; Allendorf, M. D.; Solomon, E. I. *J. Am. Chem. Soc.* **1989**, *111*, 4009. (e) Garribba, E.; Micera, G. *J. Chem. Educ.* **2006**, *83*, 1229.
(31) Neese, F. *J. Phys. Chem. Solids* **2004**, *65*, 781.
(32) (a) Schaefer, A.; Horn, H.; Ahlrichs, R. *J. Chem. Phys.* **1992**, *97*, 2571. (b) The Ahlrichs auxiliary basis sets were obtained from the TurboMole basis set library at ftp.chemie.uni-karlsruhe.de/pub/jbasen. (c) Eichkorn, K.; Treutler, O.; Ohm, H.; Haser, M.; Ahlrichs, R. *Chem. Phys. Lett.* **1995**, *240*, 283. (d) Eichkorn, K.; Weigend, F.; Treutler, O.; Ahlrichs, R. *Theor. Chem. Acc.* **1997**, *97*, 119.
(33) (a) Becke, D. A. *Phys. Rev. A* **1988**, *38*, 3098. (b) Perdew, J. P. *Phys. Rev. B* **1986**, *33*, 8822. (c) Perdew, J. P. *Phys. Rev. B.* **1986**, *34*, 7406. (d) Kendall, R. A.; Früchtl, H. A. *Theor. Chem. Acc.* **1997**, *97*, 158.
(34) Kahn, O.; Briat, B. *J. Chem. Soc., Faraday Trans 2* **1976**, *72*, 268.
(35) Onofrio, N.; Mouesca, J.-M. *Inorg. Chem.* **2011**, *50*, 5577. Rodríguez-Fortea, A.; Alemany, P.; Alvarez, S.; Ruiz, E. *Inorg. Chem.* **2002**, *41*, 3769.
(36) Bianchi, A.; Fallani, D. G.; Ghilardi, C. A.; Sacconi, L. *J. Chem. Soc., Dalton Trans.* **1973**, 641.
(37) (a) Reinen, D.; Friebel, C. *Inorg. Chem.* **1984**, *23* (7), 791. (b) Arriortua, M. I.; Mesa, J. L.; Rojo, T.; Debaerdemaeker, T.; Beltrán-Porter, D.; Stratemeier, H.; Reinen, D. *Inorg. Chem.* **1987**, *27*, 2976.
(38) (a) Bersuker, I. B. *The Jahn–Teller Effect*; Cambridge University Press: Cambridge, U.K., 2006. (b) Harrison, D.; Kennedy, D.; Hathaway, B. *Inorg. Nucl. Chem. Lett.* **1981**, *17*, 87.
(39) Worm, K.; Chu, F.; Matsumoto, K; Best, M. D.; Lynch, V.; Anslyn, E. V. *Chem.—Eur. J.* **2003**, *9*, 741.
(40) Noro, S.-i.; Akutagawa, T.; Nakamura, T. *Chem. Commun.* **2010**, 4619.

(41) Blake, A. J.; Devillanova, F. A.; Garau, A.; Harrison, A.; Isaia, F.; Lippolis, V.; Tiwary, S. K.; Schröder, M.; Verani, G.; Whittaker, G. *J. Chem. Soc., Dalton Trans.* **2002**, 4389.
(42) Emsley, J.; Arif, M.; Bates, P. A.; Hursthouse, M. B. *J. Chem. Soc., Dalton Trans.* **1989**, 1273.
(43) Machura, B.; Małecki, J. G.; Świtlicka, A.; Nawrot, I.; Kruszynski, R. *Polyhedron* **2011**, *30* (5), 864.
(44) (a) Fujisawa, K.; Kanda, R.; Miyashita, Y.; Okamoto, K.-i. *Polyhedron* **2008**, *27*, 1432. (b) Machura, B.; Świtlicka, A.; Kruszynski, R.; Kusz, J.; Penczek, R. *Polyhedron* **2008**, 2513.
(45) Zhai, B.; Shen, W.-Z.; Chen, X.-Y.; Song., H.-B.; Shi, W.; Cheng, P. *Inorg. Chem. Commun.* **2006**, *9*, 1293.
(46) (a) Melnik, M. *Coord. Chem. Rev.* **1981**, *36*, 1. (b) Harcourt, R. D.; Skrezenek, F. L.; Maclagan, R. G. A. R. *J. Am. Chem. Soc.* **1986**, *108* (18), 5403. (c) De Loth, P.; Cassoux, P.; Daudey, J. P.; Malrieu, J. P. *J. Am. Chem. Soc.* **1981**, *103* (14), 4007.
(47) Grant, C. M.; Stamper, B. J.; Knapp, M. J.; Folting, K.; Huffman, J. C.; Hendrickson, D. N.; Christou, G. *J. Chem. Soc., Dalton Trans.* **1999**, 3399.